COMPARATIVE ANALYSIS OF ESTIMATED LONGSHORE SEDIMENT TRANSPORT RATES WITH RIVER AND DREDGING FLUXES IN THE SAVANNAH CHANNEL

by

OSCAR JULIAN VILLEGAS GUTIERREZ

(Under the Direction of Dr. Matthew V. Bilskie and C. Mark Risse)

ABSTRACT

Determining the relative contributions of inland and marine sediment sources is essential for accurately predicting and managing sedimentation in harbors. The Savannah River navigation channel is characterized by strong tidal currents, which move water and sediments in and out of the system with the tides. A hydrodynamic-wave model was developed to accurately reproduce water surface elevations and tides, which were then used to compute longshore sediment transport (LST) at locations south of the outer Savannah River channel near Tybee Island. Southward transport rates were 485,864 m^3/year at East Tybee Island and 728,080 m^3/year at Southeast Tybee Island. In contrast, North Tybee Island exhibited a northward transport rate of 144,601 m^3/year, confirming a previously reported local reversal. The computed rates align with previous LST estimates but are significantly lower than dredging records. This discrepancy suggests reduced sediment availability south of the channel, likely due to sediment trapping in the channel.

INDEX WORDS: Longshore sediment transport, CERC, Savannah Channel, ADCIRC+SWAN.

COMPARATIVE ANALYSIS OF ESTIMATED LONGSHORE SEDIMENT TRANSPORT RATES WITH RIVER AND DREDGING FLUXES IN THE SAVANNAH CHANNEL

by

OSCAR JULIAN VILLEGAS GUTIERREZ

B.S., Francisco Jose de Caldas District University, Colombia, 2009

A Thesis Submitted to the Graduate Faculty of The University of Georgia in Partial Fulfillment of the Requirements for the Degree

MASTER OF SCIENCE

ATHENS, GEORGIA

2024

COMPARATIVE ANALYSIS OF ESTIMATED LONGSHORE SEDIMENT TRANSPORT

RATES WITH RIVER AND DREDGING FLUXES IN THE SAVANNAH CHANNEL

by

OSCAR JULIAN VILLEGAS GUTIERREZ

Major Professor:	Matthew V. Bilskie
	C. Mark Risse
Committee:	Clark Alexander

Electronic Version Approved:

Ron Walcott
Vice Provost for Graduate Education and Dean of the Graduate School
The University of Georgia
December 2024

DEDICATION

A hat full of dreams.

ACKNOWLEDGEMENTS

I would like to extend my deepest gratitude to Dr. Matthew Bilskie and Dr. Mark Risse for their warm welcome to the University of Georgia and the COAST Lab, as well as for their invaluable support throughout my time here.

A heartfelt thank you goes to all my COAST Lab mates—Sheppard, Becca, Ada, Aditya, Bobby, Caraline, Grant, Nashid, Ebrahim, Lina, Alex, Saeid, and Hunter. Your support and the camaraderie we shared made this journey truly special.

I'd also like to thank Dr. Clark Alexander for his insightful guidance and clever advice throughout this thesis. Your expertise and encouragement were crucial to my progress.

Special thanks to my "sediment team"—Dr. Rhett Jackson, Caleb Systma, Ellis Kalaidjian, and Margaret Kurth. Your shared thoughts and resources have been invaluable in exploring this exciting topic.

I would also like to acknowledge my family for their unwavering support. To my wife and daughter, thank you for walking with me on this journey without hesitation.

This work was supported by the US Army Corps of Engineers Engineering With Nature® Initiative through Cooperative Ecosystem Studies Unit Agreement W912HZ2020031.

TABLE OF CONTENTS

LIST OF TABLES

LIST OF FIGURES

CHAPTER 1 INTRODUCTION

As sea levels continue to rise and the demand for resilient coastal infrastructure grows, the need for sediment resources has become increasingly urgent as sediment dynamics significantly influence crucial aspects of modern society, including water quality, navigation, and recreational areas, and have profound effects on estuaries, deltas, and coastal zones (Ouillon, 2019).

Coastal regions are confronted with the dual challenges of erosion and maintenance of navigational channels, underscoring the critical importance of effective sediment management (Elko et al., 2021). In response, there has been a growing emphasis on the reuse of dredged sediment in a manner that benefits ecosystems and communities (Kress et al., 2016; USACE, 2015). The U.S. Army Corps of Engineers (USACE) has been at the forefront of efforts to expand the beneficial use of dredged material, recognizing its potential to support environmental restoration, shoreline protection, and broader resilience goals (USACE, 2023).

Longshore sediment transport (LST) plays a key role in shaping coastal morphology, and understanding the local wave climate and sediment movement is crucial for designing effective projects, developing management strategies, and assessing erosion risks (Trombetta et al., 2020). Accurate estimates of LST rates and their distribution across the surf zone are crucial for coastal engineering applications, as they are essential for predicting beach evolution near coastal structures, projecting renourishment requirements, and determining sedimentation rates in navigation channels (Smith et al., 2009).

The Savannah River navigation channel is characterized by strong tidal currents that move water and sediment in and out of the system with the rise and fall of tides (Defne et al., 2011). An integrated hydrodynamic and wave model was employed to simulate nearshore waves and currents LST was estimated by using the empirical CERC formula. This research aims to address the following research questions:

- What are the longshore sediment transport rates for a normal year in the study area?
- How do estimated longshore sediment transport rates compare to river and dredging fluxes?

To address these questions, this thesis is organized as follows: A literature review regarding sediment characteristics in the area and different approaches to estimating LST. Then, the hydrodynamic wave and sediment model is provided, then the results are compared with available LST studies and Savannah Channel dredging records. Discussion and conclusions are based on the analysis of modeled results and measured data.

In conclusion, this study aims to provide a comprehensive comparative analysis of estimated LST rates with river and dredging fluxes in the Savannah Channel. By integrating empirical methods and hydrodynamic modeling, this research enhances our understanding of sediment dynamics in this pivotal coastal region, ultimately contributing to more effective sediment management and coastal protection strategies.

It is crucial to acknowledge that while there are various methodologies for estimating LST, comparisons of such results with dredging records and river inputs must be approached with consideration of the methods used to obtain the data and the specific purposes of the comparison. Each method has its own set of assumptions and limitations and the contextual differences between natural sediment transport processes and human-induced changes must be carefully evaluated.

CHAPTER 2 LITERATURE REVIEW

2.1. Port of Savannah and Navigation Channel

The Port of Savannah, with its primary emphasis on container traffic, serves as the focal point for one of the most extensive logistics clusters in the United States. From 2017 to 2021, It has been nation's fourth-busiest container port (USDOT, 2024). It is also the second-busiest along the Atlantic coast, granting convenient access to approximately 44% of U.S. consumers within a span of 2-3 days (Carse & Lewis, 2020). The navigation channel stretches around 37 miles, starting from Savannah Harbor near the City of Savannah, flowing downstream to the entrance located just east of Fort Pulaski on Cockspur Island, and finally leading out to the Atlantic Ocean through Tybee Roads (Smith et al., 2008).

The total length of the harbor is divided into two main sections: the inner channel, which extends 21.3 miles upstream from the channel entrance near Fort Pulaski National Monument, and the outer channel, which extends approximately 17 miles into the ocean from the same entrance (USACE, 2012). The U.S. Army Corps of Engineers (USACE) designates locations along the Savannah Channel by their linear distance from the channel entrance, which is known as Station (Sta) 0+000. Consequently, the entire navigation channel ranges from Sta 112+500 (112,500 feet upstream) to Sta -90+000 (90,000 feet offshore) (see Figure 1).

The historical dredging activities in Savannah Channel reflect ongoing efforts to maintain and deepen the navigation channel. The Savannah River navigation channel was initially deepened in 1912 from 21.5 ft to 26 ft below mean low water (MLW) to accommodate larger vessels. Subsequent deepening projects increased the channel depth to 30 ft MLW in 1936 and to

36 ft MLW in 1945. In 1972, the channel was both widened and deepened to 40 ft MLW, and in 1994, the authorized depth was further increased to 44 ft MLW (Smith et al., 2008). More recently, the Savannah Harbor Expansion Project (SHEP) took place between 2015 and 2022, further deepening the channel to 47 feet to accommodate larger vessels and enhance the port's capacity (USACE, 2024a). This effort facilitates the passage of larger containers through the channel and signifies the port's anticipation of continued expansion and development (Ramos, 2014).

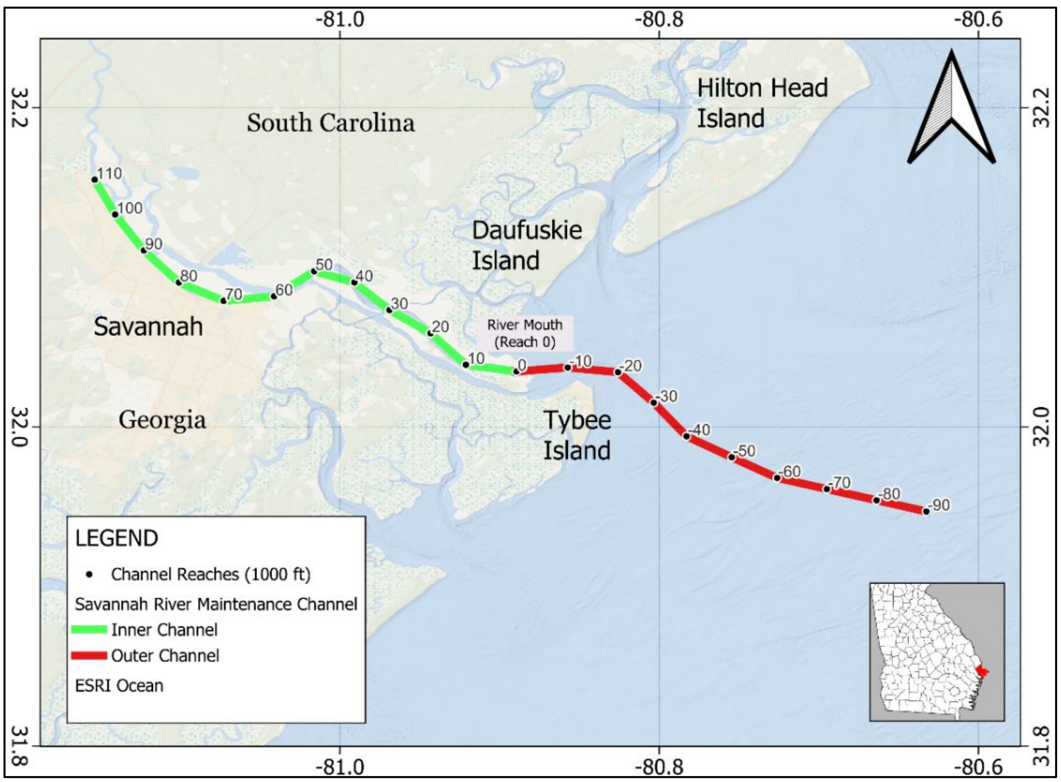

Figure 1 Savannah River Channel

The Port of Savannah employs two primary types of dredging operations: maintenance dredging and new work dredging. Maintenance dredging is a routine activity designed to ensure the channel's navigational depth by periodically removing accumulated sediment, thereby preventing shoaling (USACE, 2024b). In contrast, new work dredging is conducted to increase the channel depth to accommodate larger vessels, as previously mentioned.

It has been estimated that the Savannah harbor dredges approximately $5.6 * 10^6$ m^3/year (USACE, 2020). The Savannah District provided a total of 10 years (Jan 2013 – Dec 2022) of daily dredge records. A total of $53.6 * 10^6$ m^3 of sediment was dredged between 2013 and 2022, with 76% sourced from the inner channel and 24% from the outer channel. Of this total, 61% ($32.6 * 10^6$ m^3) was attributed to maintenance dredging, while 39% ($21.4 * 10^6$ m^3) was related to new work dredging associated with the deepening of the channel for the SHEP.

2.2. Longshore Sediment Transport (LST)

Determination of relative contributions of inland and marine sources of sediment in estuaries is essential for accurately predicting and managing sedimentation in harbors (Mulholland & Olsen, 1992). Among various oceanographic factors like winds, tides, currents, and near-shore waves exert a significant influence on the coastal geomorphology. Sediment transport along the surf-zone is usually generated by longshore currents generated by the breaking waves (Chempalayil et al., 2014).

For the present study, longshore transport refers to the *"cumulative movement of beach and nearshore sand parallel to the shore by the combined action of tides, wind, and waves and the shore-parallel currents produced by them"* (Seymour, 2005). In the surf zone, sediment primarily undergoes mobilization due to oscillatory wave-induced flows. When the wave angle relative to the shoreline is less than 90 degrees, sediment is transported by a longshore wave-induced current. Additionally, sediment movement occurs both onshore and offshore through the combined action of asymmetric wave-induced flows, undertow, and infragravity waves, which eventually creates beach features (Williams et al., 2007). Additionally, the depth of the underwater terrain, known as the bathymetric depth, plays a crucial role in determining the erosion, suspension, and deposition patterns of sediments within the given area (Pandoe & Edge, 2008).

Direct measurements, empirical formulas, and inference from observed large scale changes in shorelines are some of the multiple approaches existing for estimating LST rates (Esteves et al., 2009). When estimating LST using empirical formulas, methodologies are classified into dimensional analysis, force-balance, and energetic methods, with the latter being sub-classified into energy flux and stream power approaches (Tomasicchio et al., 2013).

The concept of the depth of closure (DoC) is intricately connected to nearshore sediment dynamics, as evidenced by multiple studies. Aragonés et al. (2018) identified DoC as the point where sediment size decreases with increasing depth to a specific depth, where it increases briefly before decreasing again. This change in sediment size trend marks the DoC, reflecting the limit of significant sediment transport due to wave and tidal influences. This emphasizes that sediment movement plays a crucial role in defining the DoC.

Further reinforcing this connection, the study by Hudson et al. (2022) discusses how wave asymmetry influences sediment transport across the nearshore profile. The authors demonstrated that the DoC is not merely a theoretical boundary but a dynamic limit where sediment transport diminishes significantly. Furthermore, Valiente et al. (2019) demonstrated that significant sediment transport can occur beyond the typical DoC during extreme events, challenging the notion that embayed beaches are closed sediment cells. This finding underscores the dynamic nature of sediment transport and its impact on the DoC, thereby reinforcing the idea that the DoC is closely related to the location where sediment movement ceases to be significant.

2.2.1. LST empirical formulas

While LST prediction is still challenging, several empirical equations have been proposed by a variety of authors. The empirical equations encompass a wide range of parameters that influence sediment transport, including wave characteristics, nearshore current velocities, sediment properties, and coastal geomorphology. In general, the parameters used in LST formulas are significant wave height at the breaker point (H_{sb}), peak spectral wave period (T_P), wave angle at breaking (α_b), and the size of sediment particles (mainly D_{50}) (Shaeri et al., 2020). Such equations are presented as follows:

CERC formula: This method assumes that the longshore transport rate Q is influenced by the longshore component of energy flux within the surf zone. To approximate this flux, it is assumed that energy flux is conserved in shoaling waves, applying small-amplitude wave theory, and the energy flux relationship is evaluated specifically at the breaker position (CERC, 1984) (USACE, 2002a).

The CERC equation estimates gross LST, defined as the total amount of littoral drift moving right and left past a shoreline point over a period. It also defines the net longshore transport rate as the difference between the drift moving updrift and downdrift within the same time frame (CERC, 1984).

It considers the alongshore component of wave energy to be the influencing factor (Equation 1):

$$Q = k_{\mathrm{CERC}}\left(\frac{\rho\sqrt{g}}{16\sqrt{\gamma_b}(\rho_s-\rho)(1-p)}\right)H_{sb}^{5/2}\sin(2\alpha_b) \qquad 1$$

Q = the LST volumetric rate (m^3/s); g = the gravitational acceleration (m^2/s); γ_b = the wave breaking index ($\gamma_b = H_{sb}/h_b$); h_b = the depth at breaker point (m); ρ_s = the sediment particle's bulk density (kg/m^3, and mostly taken as 2,650 kg/m^3); ρ = the ambient water density (kg/m^3, and mostly taken as ~1,025 kg/m^3 for seawater); p = the porosity of the sediment particles (mostly taken as ~0.40); H_{sb} = the significant wave height at breaker point (m); and α_b = the incident angle of waves at breaker point (deg. or rad.). k_{CERC} is an empirical coefficient (Equation 2)

$$k_{\text{MH,CERC}} = \left[2{,}232.7\left(\frac{H_{sb}}{L_o}\right)^{1.45} + 4.505\right]^{-1} \quad 2$$

where L_0 (in m) = the deep-water wavelength = $g\left(T_p^2\right)\big/_{2\pi}$

Kamphuis's Formula: Kamphuis (1991) developed his equation based on dimensional analysis of small-scale laboratory data. Later on, Mil-Homens et al. (2013) proposed an improvement on Kamphuis's Formula as follows (Equation 3):

$$Q = k_{(\text{MH,KPH})} H_{sb}^{2.75} T_P^{0.89} m_b^{0.86} D_{50}^{-0.69} \sin^{0.5}(2\alpha_b) \quad 3$$

For this equation, m_b is the beach slope within the surf zone (where $m_b=h_b/x_b$ and x_b is the horizontal distance from shoreline to the break point), and D_{50} is the sediment particle size (m). $k_{MH,KPH}$ (in the unit of m$^{0.94}$ s$^{-1.89}$) is defined in equation 4 :

$$k_{(\text{MH,KPH})} = \frac{0.149}{(\rho_s - \rho)(1 - p)} \quad 4$$

Smith et al. (2009) conducted experiments at the Large-scale Sediment Transport Facility (LSTF) at the U.S. Army Engineering Research and Development Center to evaluate the performance of the CERC and Kamphuis equations in predicting LST rates. Using data from physical experiments, they found that the CERC equation tended to overestimate LST rates, particularly for spilling breakers. However, when calibrated for specific breaker types, it performed more accurately. On the other hand, the Kamphuis equation, which accounts for wave period, beach slope, and sediment size, consistently produced more accurate predictions, aligning closely with the measured data (Smith et al., 2009).

GENESIS formula: GENESIS equation proposed by the USACE (Demirbilek & Linwood, 2002) (Equation 5):

$$Q = \left(H^2 C_g\right)_b \left[a_1 \sin(2\theta_b) - a_2 \cos(\theta_b)\left(\frac{\partial H_b}{\partial x}\right)\right]$$

$$a_1 = \frac{K_1}{16\left(\frac{\rho_s}{\rho} - 1\right)(1-n)(1.416)^{5/2}} \qquad 5$$

$$a_2 = \frac{K_2}{8\left(\frac{\rho_s}{\rho} - 1\right)(1-n)m(1.416)^{7/2}}$$

Where H=wave height; C_g=wave group velocity; ρ=density of water; ρ_s=sediment density; n=sediment porosity; m=beach slope; and subscript b denotes wave conditions at breaking. Wave angle, Ɵ, is measured relative to the local shore-normal vector. K_1 and K_2=empirical calibration factors; for the case of K_2=0 or $\partial H_b/\partial x$=0.

Bayram et al.'s Formula: Bayram et al. (2007) considers the combined effects of longshore current and a fraction of wave energy. Bayram et al.'s Formula was also modified by Mil-Homens et al. (2013) as shown in equation 6: .

$$Q = \frac{k_{(\mathrm{MH,B})}}{(\rho_s - \rho)(1-p) g w_s} F_b \overline{V} \qquad 6$$

$$k_{(\mathrm{MH,B})} = \left[786{,}200\left(\frac{H_{sb}}{L_o}\right)^{1.283} + 1{,}672.2\right]^{-1} \qquad 7$$

F_b represents the wave energy flux (after breaking), $\bar{V}$ is the representative longshore current velocity, averaged across the surf zone width, H_{sb} = the significant wave height at breaker point (m), and L_0 (m) = the deep-water wavelength.

Tomasicchio et al.'s Formula: Tomasicchio et al. (2013) revised an equation originally used for designing reshaped berm breakwaters, by introducing a modified (armor) stability number ($N_s^{(**)}$) (Equation 8):

$$Q = (S_N D_n 50^3)/T_m \quad 8$$

Where T_m = the mean wave period, S_N = the number of rock units moved due to one wave action, and D_{n50} nominal particle size.

van Rijn formula: van Rijn (2014) equation proposed a dimensionally homogenous formula for a wide range of particle sizes between 0.1 and 100 mm (i.e., sand, gravel, and shingle). The author also considered the impact of swell waves, revealing that regular swell waves result in a higher (LST) rate when compared to irregular wind waves of similar wave height (Equation 9).

$$Q = \frac{0.00018\sqrt{g}}{1-p} K_{\text{swell}}\, H_{sb}^{3.1} m_b^{0.4} D_{50}^{-0.6} \sin(2\alpha_b) \quad 9$$

When describing this formula, Shaeri et al. (2020) it clarifies van Rijn's K_{swell} values which is a coefficient related to p_{swell} (percentage of low-period swell waves of all the wave records) (Equation 10):

$$K_{\text{swell}} = \text{MAX}\,1, \text{MIN}\left[1.5, 1.5 - 10\left(\frac{H_{sb}}{L_0} - 0.01\right)\right] \quad 10$$

Shaeri et al.'s Formula: Shaeri et al. (2020) considered physical arguments and multi-variable regression analysis to propose these equations (Equation 11, Equation 12):

$$Q = \frac{3 \times 10^{-4}}{\Delta(1-p)} H_{sb}^2 T_p^{0.8} D_{50}^{-0.25} \sin^{0.6}(2\alpha_b) \quad 11$$

$$Q\frac{1}{H_{sb}^3/T_p} = \frac{3 \times 10^{-4}}{\Delta(1-p)} \left(\frac{H_{sb}}{L_0}\right)^{-0.9} \left(\frac{H_{sb}}{D_{50}}\right)^{0.2} \sin^{0.5}(2\alpha_b) \quad 12$$

Where H_{sb} = significant wave height at beaker point, T_p = peak wave period, D_{50} = particle size diameter, α_b = wave angle at breaker point, and L_0 = offshore wavelength.

Empirical methods are useful in calculating LST because they provide a straightforward, simplified approach that relies on readily measurable parameters, making them accessible and practical for rough initial estimates. While these methods have significant advantages, they are also prone to error due to omitting key factors such as wave period and sediment size. For instance, CERC formula is relatively simple and widely used; however, it lacks accuracy in accounting for sediment size and wave period. Kamphuis's formula represents an improvement on the preceding formulas by including sediment size and beach slope, though it requires more data. Bayram et al.'s formula is more comprehensive but complex and assumption-heavy. Van Rijn's formula handles a wide range of sediment sizes but is more difficult to use due to its inclusion of swell wave effects. Tomasicchio et al.'s formula is detailed but overly complex for typical LST applications (Shaeri et al., 2020). Moreover, the need for calibrating the sand transport coefficient introduces substantial uncertainty, affecting the reliability of the results up to 100% (Barua, 2015).

The CERC formula is the method employed in the present analysis for estimating LST. Hydrodynamics and wave modelling provide the essential inputs for the CERC equation, including the significant wave height at the breaker point (Hsb), the wave angle at breaking (αb), and the wave energy flux (USACE, 2002a). In addition, the CERC equation has been successfully calibrated for sandy beaches, where the sediment grain size and beach slope exert less influence on transport rates (Trombetta et al., 2020).

2.2.2. LST numerical modeling

The utilization of computational hydrodynamic/sediment transport models involves numerically solving one or more governing differential equations, which include continuity, momentum, and energy equations for fluid, alongside the differential equation for sediment continuity (Papanicolaou et al., 2008).

An LST semi-empirical model which combined sediment concentration profile data obtained from field measurements with predictions of hydrodynamic parameters was developed by Esteves et al. (2009). The hydrodynamic inputs were wave height, period, and breaker type, and the results were used in sediment transport processes simulation. LST rates obtained were validated against field data from various locations, showing better performance over extended periods compared to traditional bulk LST formulas such as the CERC and Kamphuis equations (Esteves et al., 2009).

Georgiou and Schindler (2009) attempted to validate CERC empirical equation through historical data and field observations of sediment deposition and erosion patterns along barrier islands. They employed a combination of wave forecasting, wave transformation, and sediment transport equations to simulate sediment dynamics. These simulations revealed significant seasonal and storm-induced variations in sediment transport, highlighting the influence of wave direction and intensity on coastal sediment dynamics. The integration of numerical models, such as SWAN (Booij et al., 1999b), allowed them to predict sediment transport trends to further predict erosion and deposition of the Chandeleur Islands barrier island system (Georgiou & Schindler, 2009).

The three studies share a common focus on evaluating LST methods, emphasizing the comparison between empirical formulas (mostly CERC equation) and actual modeling results. Despite its widespread use, these studies also showed that the CERC formula often overpredicts LST rates unless calibrated with site-specific data.

To model sediment transport, Pandoe and Edge (2008) proposed an advancement in ADCIRC (Luettich et al., 2004) that involves the integration of an extended transport module, which is now noninteractively coupled with the SWAN wave model. This novel approach allows for the estimation of surface wave effects on sediment transport mechanisms. The model has been successfully employed to assess the transport of contaminated material (sediment) in Matagorda Bay, Texas, under natural wind and tide conditions. The model developed by the authors is for cohesive materials as it was developed for that specific Bay that contained cohesive sediment.

The hydrodynamics and sediment dynamics of the Chincoteague Inlet system located along the northern Eastern Shore of Virginia were analyzed using the Delft3D model. The model integrated flow, wave interactions, sediment transport, and morphologic feedback to understand regional sediment transport pathways. The model revealed that finer sands are transported around the spit, highlighting the significant impact of wave-induced processes on the overall sediment transport dynamics in the area (Georgiou et al., 2023).

A LST analysis for the sandy coast of Boumerdes, Algeria was presented by Salem Cherif et al. (2019) which included empirical formulas, field measurements and numerical simulations using MIKE 21/3 FM coupled model. The study applied four empirical formulas: CERC (1984), Kamphuis (1991), Modified Kamphuis (2013), and Van Rijn (2014) and field measurements using sediment traps to validate these formulas. Wave transformations, currents and sediment transport and hydrodynamic modeling using MIKE 21/3 FM was performed to validate field data. The MIKE 21/3 FM model simulations showed that wave-induced currents increased sediment transport from east to west along the Boumerdes coast, particularly in areas exposed to strong wave energy (Salem Cherif et al., 2019).

Wave modeling and sediment transport analysis was performed in the Yucatan peninsula. The study utilized the MIKE 21 SW model to simulate wave conditions along the northern coast of the peninsula, using 12 years of hindcast data from the WAVEWATCH III model. The sediment transport model used in the study was LITDRIFT, which is part of the MIKE 21/3 suite developed by DHI. This model calculates total sediment transport by summing bedload and suspended sediment transport, based on wave conditions from the MIKE 21/3 SW model. The model employed a constant beach profile and sediment characteristics, with wave data used to drive the transport calculations (Appendini et al., 2012).

2.3 Sediment Dynamics in the Georgia Coast

The Georgia Bight islands rely on net LST from the north to the south and most islands are eroding at the northern end and accreting at the southern end (Meyer et al., 2016). However, interpreting a predominant LST direction becomes challenging due to the presence of tidal processes that along with the longshore processes contribute to shaping the coast. In generalized field studies, prevailing southward sediment transport direction has been observed, interspersed with frequent local reversals (van Gaalen et al., 2016).

As posited by Smith et al. (2008), shore-parallel tidal and wind-driven currents in the study area enhance sediment transport. In the nearshore zone, breaking waves generate bottom shear stress and turbulence, mobilizing sediments that are transported along the shoreline by longshore currents. Tidal and wind-driven flows further complicate these dynamics. Offshore, waves primarily stir sediments near the seabed, while ocean circulation currents dominate their transport.

On the northern end of Tybee Island, a northward drift direction has been reported as an exception to the prevailing southward sediment transport direction. Oertel et al. (1985) found that this northward sediment transport is ephemeral and conflicts with the generalized drift direction observed in the area.

A map illustrating the direction and rate of longshore transport, created using data from various site-specific and regional studies, is presented in Figure 2.

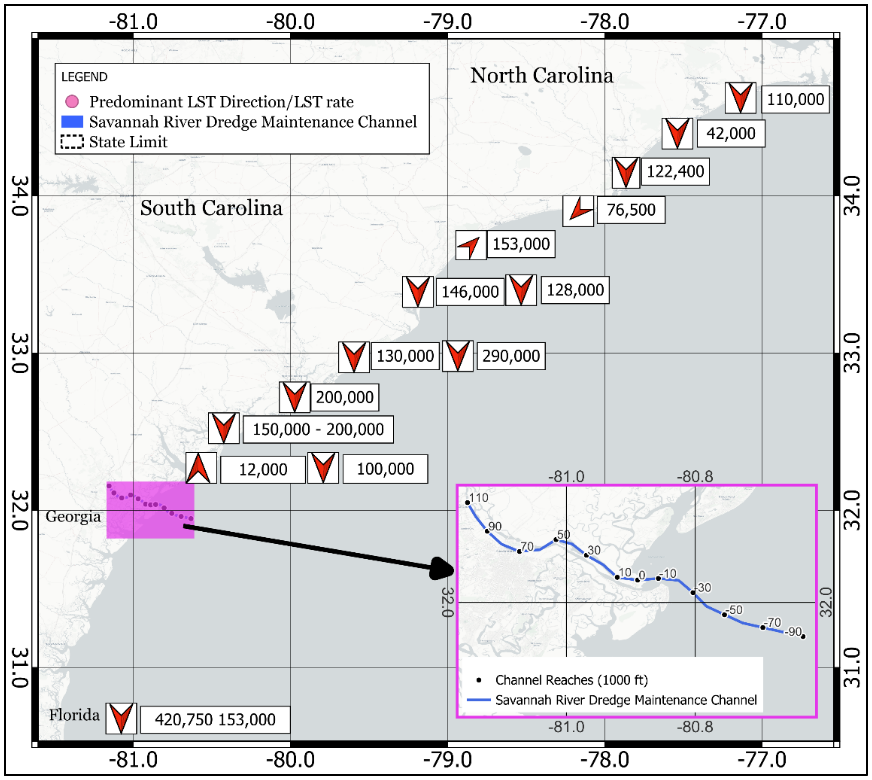

Figure 2 LST predominant direction and rate (m^3/y)
Modified from van Gaalen et al. (2016)

With the port expected to undergo further expansion, Smith et al. (2008) evaluated the impact of the Savannah Harbor Deep Draft Navigation Project on the shores of Tybee island. Before the deepening of Savannah Channel and the construction of jetties, sediment transport patterns around Tybee Island were dominated by natural processes. These included tidal currents, wave action, and riverine sediment supply, which together created a balanced system of erosion and accretion. The shoreline was relatively stable, with natural features like the northern bulge of Tybee Island maintained by uninterrupted sediment pathways. This natural sediment dynamic was significantly altered by the subsequent deepening of the channel and the construction of jetties, leading to the disrupted sediment transport patterns observed in the post-project period.

The feasibility of nearshore placement for beneficial use of dredged material to nourish the littoral zone, including hydrodynamic, wave and sediment transport modeling were used by Gailani and Smith (2014) to assess the dynamics of dredged material. The Advanced CIRCulation (AdCirc) model was used for hydrodynamic simulations, and the STeady-state spectral Wave model (STWave) was used for wave conditions. GTran, a sediment transport model, was developed to assess transport pathways and trends for multiple placement scenarios. In addition to nearshore placement recommendations, the study found that the predominant longshore transport direction is from north to south. This transport direction is crucial for understanding how sediment moves along the shoreline and the impact of various sediment management practices.

Specifically for the Savannah Harbor Navigation Channel, the major sources of sediment are the Savannah River and offshore sediments carried into the harbor by tidal currents. The sediment supplied by the Savannah River is primarily fine silt and clay. The bed load material transported by the Savannah River is deposited in the extreme upper reaches of the Savannah Channel. The shoaling in the lower channel is primarily due to sand carried into the channel from the ocean by strong bottom flood currents (USACE, 2009).

2.4 Longshore Sediment Transport in Georgia

The LST rates in Georgia exhibit considerable variability, with rates ranging between 100,000 cubic meters per year (m^3/y) and 300,000 m^3/y (van Gaalen et al., 2016). Local variations and reversals in transport rates are also observed. For instance, Tybee Island has reported an ephemeral northward transport direction, while the general trend is southward (Oertel et al., 1985). Olsen Associates (2002) estimated 613,000 m^3/year, as the total influx of sand material into the navigation channel. This value includes the sand material that enters the outer channel and the material in sections 0+000 to 24+000 that

2.5. Energy Spectrum

The energy flux approach, the most common method for estimating littoral sediment transport, relates the transport rate to the longshore component of wave energy flux (Komar & Inman, 1970). Energy flux, which refers to the amount of wave energy propagating from the generation area to a specific location, is calculated based on directional spectra, providing insights into the spatial distribution of wave energy across the ocean (Lucas et al., 2011) The wave energy spectrum describes the distribution of energy across different frequencies and directions of waves at a given location on the ocean surface, and is often included in coastal engineering design processes (Lobeto et al., 2022).

The present study will use energy flux analysis to gain insights into the primary direction of wave movement and the associated energy flux that drives the transport of sediment along the coastline of the study area. This approach is incorporated into the CERC formula, as explained in section 2.2.1. LST empirical formulas.

2.6 Conclusion

Dredging activities have the potential to create sediment traps and modify sediment delivery patterns, which can have significant downstream consequences. Therefore, it is essential to employ effective sediment management strategies that mitigate these negative impacts by modeling these crucial processes (Carse & Lewis, 2020).

In terms of sediment management, Georgia has increasing interest in regional sediment management (RSM) and the beneficial use of dredged material (BUDM) to address coastal challenges. Historical trends and future projections using ARIMA models suggest a growing need for sediment management in Georgia, emphasizing the importance of optimizing sediment use to sustain coastal resilience and infrastructure (Palaparthi & Briggs, 2024).

There is limited comprehensive research on LST in the State of Georgia. This is because tidal processes have a greater influence than longshore currents, which makes the interpretation of predominant LST directions challenging (van Gaalen et al., 2016). However, the prevalence of tidal processes relative to those of longshore currents in Georgia necessitates studies that focus on the interaction between these two factors. This could help elucidate the impact of tidal influences on LST and provide more accurate regional transport models.

CHAPTER 3 METHODS

3.1. Study area

The Savannah River is a major river in the southeastern United States, with a watershed spanning 27,390 km^2 in an extensive alluvial region (Figure 3). Three upstream dams constructed by the U.S. Army Corps of Engineers between 1946 and 1985 influence the river's flow and sediment content. These dams have impacted the river's discharge and the amount of sediment available downstream (Jones et al., 2017).

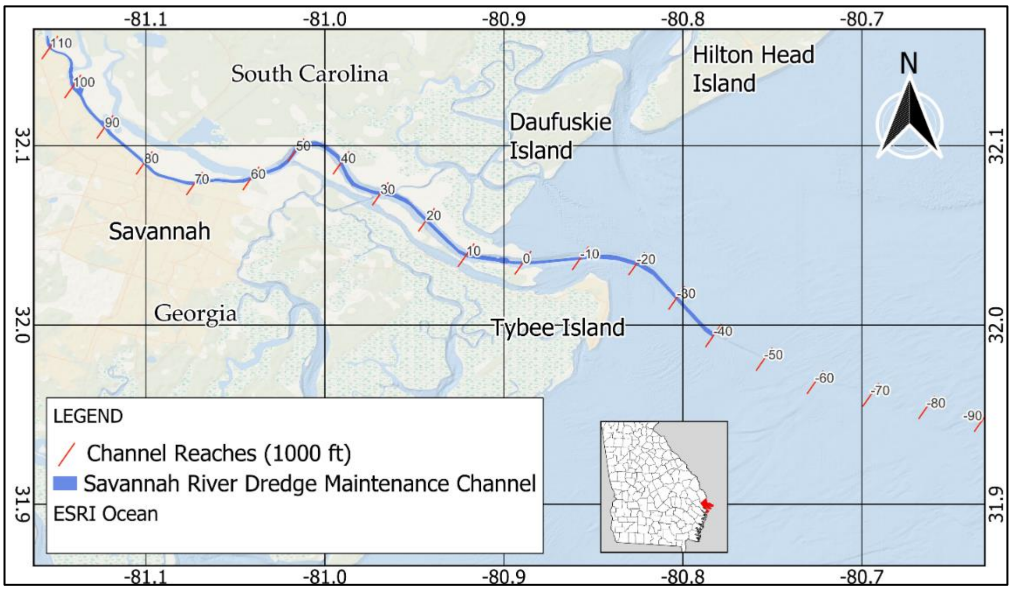

Figure 3 Study area. Savannah Harbor Navigation Channel

The study area for this research is specifically defined as the Savannah Harbor Navigation Channel. The geomorphologic area is the Lower Coastal Plain of the Atlantic Coastal Plain (ACP) physiographic province, characterized by sediments that typically encompass diverse mixtures of unconsolidated to partially consolidated sediments. Moreover, Savannah Harbor has an extensive estuarine system consisting of freshwater and salt marshes. This estuarine system, representative of other estuaries found along the Southeastern Atlantic Coast, dates back to the Holocene era (ATM, 2002).

The eastern Atlantic Coastal Plain (ACP) of the United States of America, stretching from New Jersey to northeastern Florida is characterized by emergent Pliocene and Pleistocene barrier/beach-ridge and back-barrier deposits and prominent seaward-facing scarps. The geological deposits of the lower Savannah River area (LSRA) are described in Markewich et al. (2020).

For the study area, there are two distinct geological units from the quaternary period are identified within the Holocene Shoreline Complex: Qhm and Qhi. Qhm deposits are characterized as fluvial marine and marine sediments, extending further inland along the Savannah River valley. In contrast, Qhi deposits dominate the areas around Tybee, Wassaw, and the seaward half of Ossabaw Islands. On Tybee Island, Qhi deposits reach heights of 2 to 3 meters, with oyster shells being the predominant material embedded in marine/estuarine quartz sand..

Previous research by Mulholland and Olsen (1992) indicated that the majority of the sediment found in the Savannah River estuary originates from the marine environment since estuaries often experience sediment deposition primarily composed of marine substances, which are transported inland through the circulation patterns of the estuary and involve the movement of saline water towards the landward direction along the bottom. This study reported that over 65% of the inorganic sediments found in suspended form or on the shallow bed had a marine source. Additionally, more than 74% of the organic sediments were determined to be of marine origin.

The deposits beneath this region consist of relatively young, unconsolidated sediments found in coastal plains, comprised of deposits from marshes and lagoons in the Holocene epochs of the Quaternary Period. Known as the Holocene Shoreline Complex, the primary composition of the deposits is sandy clay and sand, featuring facies of marshes and lagoons that formed during previous periods of high sea levels (GADNR, 1977).

3.2. Winds, Tides and Waves

3.2.1. Winds

The prevailing winds over the South Atlantic region are influenced by either the Azores High or a smaller anticyclone centered over the Ohio Valley, resulting in a dominant eastward wind. The streamlines reveal a southward flow of dry air from the Ohio Valley, contrasted by northward streamlines carrying warm, humid air from the Azores High. The interaction and relative positioning of these air masses shape the region's monthly climatology.

Additionally, the area's seasonal wind patterns are largely driven by shifts in the positions of the Azores-Bermuda High—also known as the "North Atlantic High/Anticyclone" or "Bermuda High/Anticyclone"—and the Icelandic Low (Blanton et al., 1985). Further analysis of the Comprehensive Ocean-Atmosphere Data Set (COADS) performed by Michel (2013), identifies five seasonal wind regimes for the South Atlantic area:

November–February (winter): Winds are stronger and southeastward (offshore) in the northern region, shifting southward and weakening in southern latitudes. A high-pressure ridge forms over the Blake Plateau, creating stronger winds on the shelf and weaker winds at the shelf break (Blanton et al., 1985) (Michel, 2013). Figure 4 and Figure 5 show the winter wind roses generated from the ERA5 dataset by the European Centre for Medium-Range Weather Forecasts (ECMWF).

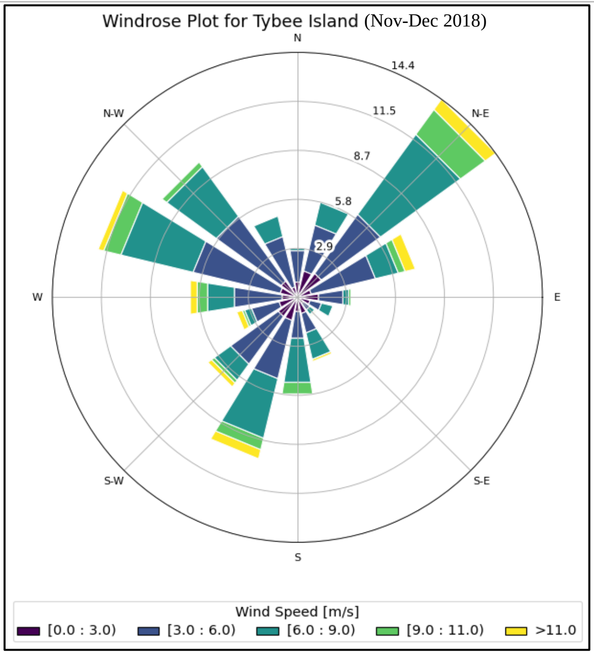

Figure 4 Windrose plot winter 2018 (Nov-Dec)

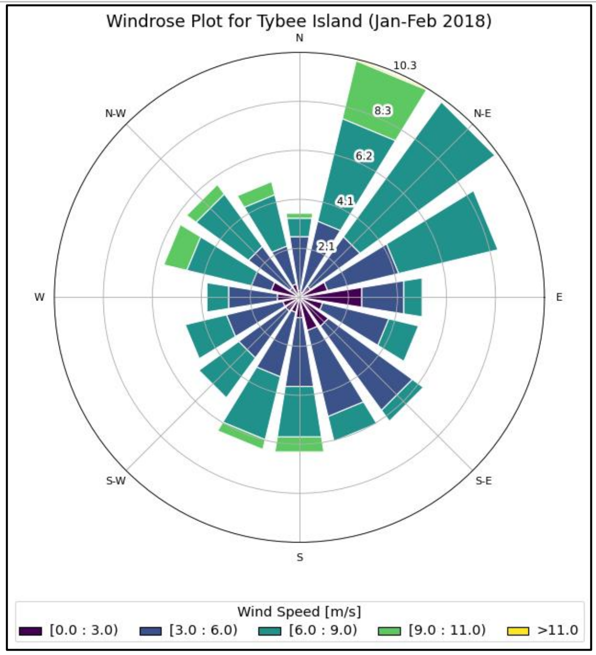

Figure 5 Windrose plot winter 2018 (Jan-Feb)

The wind roses for the winter period of 2018 indicate that the predominant direction of wind is not southeastward (offshore), as might be expected, but rather inland. However, the data also show that southward winds are predominant for this time of the year.

March–May (spring): Winds gradually shift to the east and northeast, with more organized patterns over the Blake Plateau. The high-pressure region weakens, and the ridge no longer extends into the South Atlantic (Blanton et al., 1985) (Michel, 2013). The wind rose for the spring of 2018, presented in Figure 6 illustrates the prevailing northward wind direction during this time of the year.

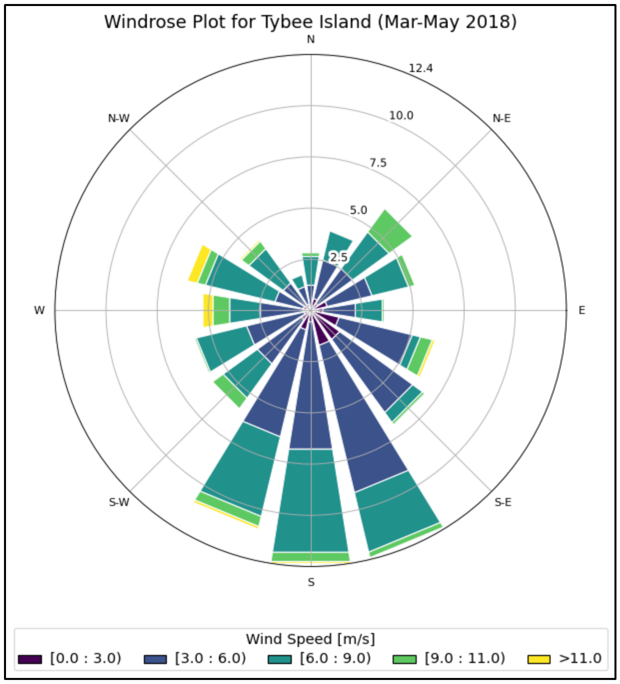

Figure 6 Windrose plot spring 2018 (mar-may)

June–July (summer): Blanton et al. (1985) and Michel (2013) describe winds westward and southwestward in southern Florida, while northward and northeastward in the northern region and over the Blake Plateau. Strongest winds occur in July, favoring upwelling along the entire eastern US coast. Wind rose generated for the summer of 2018 shows wind flowing northward, although maximum wind velocities are within 9.0 to 11.0 m/s (See Figure 7).

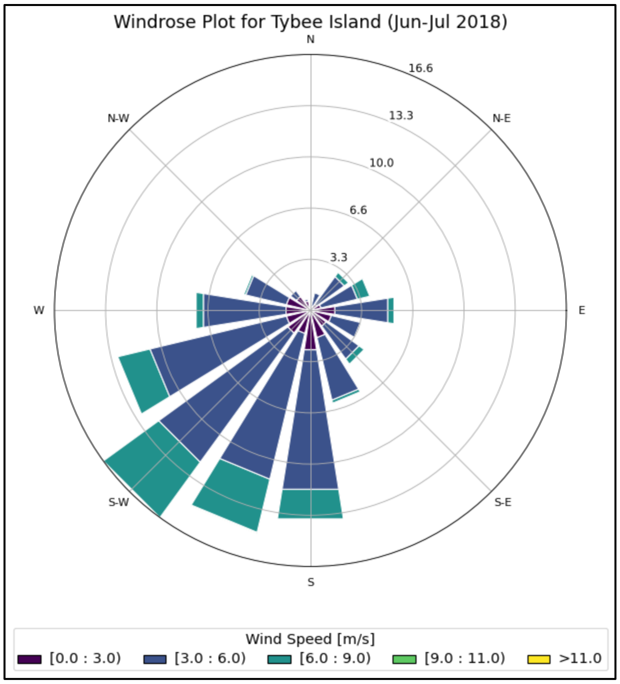

Figure 7 Windrose plot summer 2018 (Jun-Jul)

August (transitions regime): period during which the Ohio Valley High is formed, generating air streams that oppose those coming from the Azores High. The relative dominance of those opposing systems appears to control the mean circulation during this period (Blanton et al., 1985); (Michel, 2013). For this period northward winds dominate as shown in Figure 8.

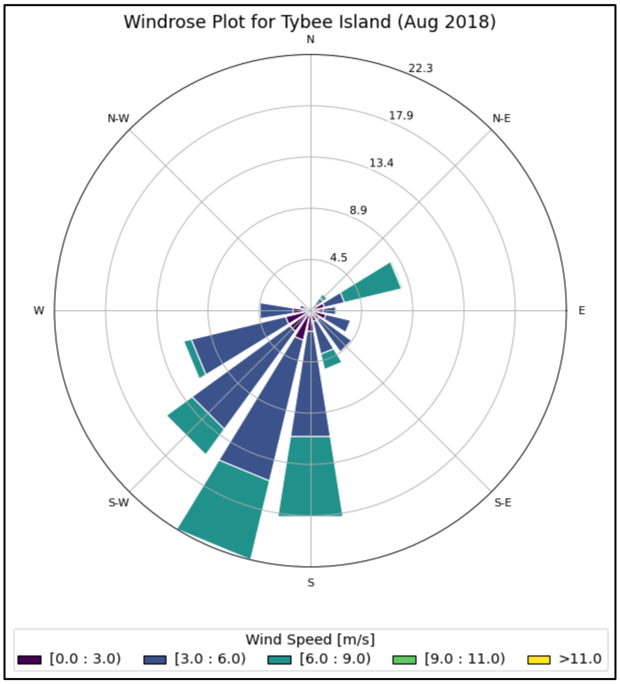

Figure 8 Windrose plot transitions period 2018 (Aug)

September–October (autumn regime): strong southwestward along-shelf wind stresses dominate, but they weaken before reaching the Blake Plateau, where the winds are primarily westward and less intense (Blanton et al., 1985) (Michel, 2013). The wind rose for autumn 2018 (see Figure 9) indicates that the prevailing wind direction is westerly, with wind velocities below 6 m/s.

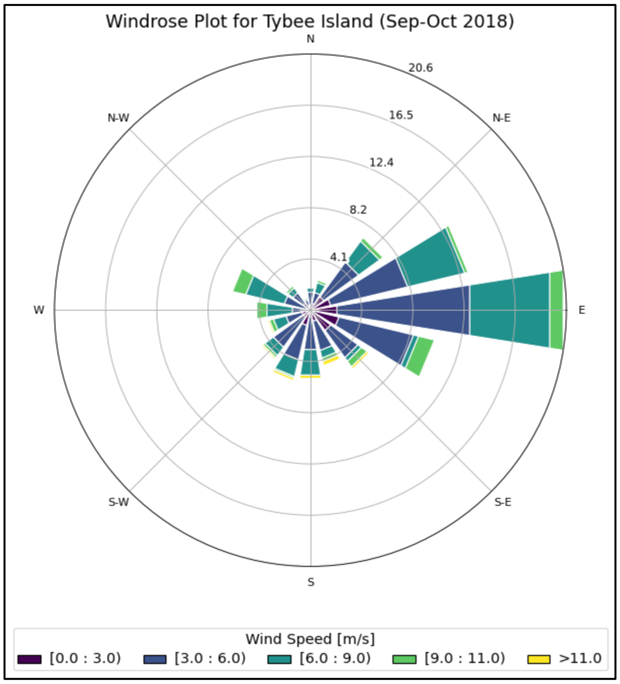

Figure 9 Windrose plot autumn 2018 (sep-oct)

2.2.2. Sea level variation

A double-peaked average seasonal cycle is observed at coastal stations from South Carolina to northern Florida. The lowest sea levels are recorded during the winter (January), with a gradual rise to a local maximum in May–June. Following this peak, sea levels decline to a secondary low in July, before increasing again to reach their highest levels in September–October (Michel, 2013). Figure 10 shows monthly variability of sea level as recorded at four NOAA coastal tidal stations along the South Atlantic Bight

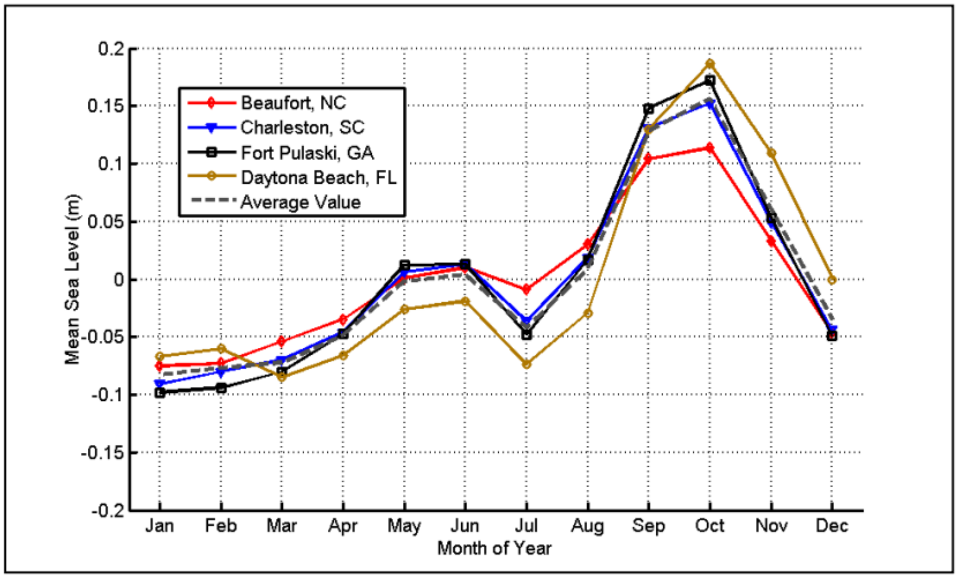

Figure 10. Monthly variability of sea level in South Atlantic NOAA stations (Michel, 2013)

The 2018 monthly average sea level, as measured by the National Oceanic and Atmospheric Administration (NOAA) in 2018, is also consistent with the trend illustrated in the preceding figure (see Figure 10 and Figure 11).

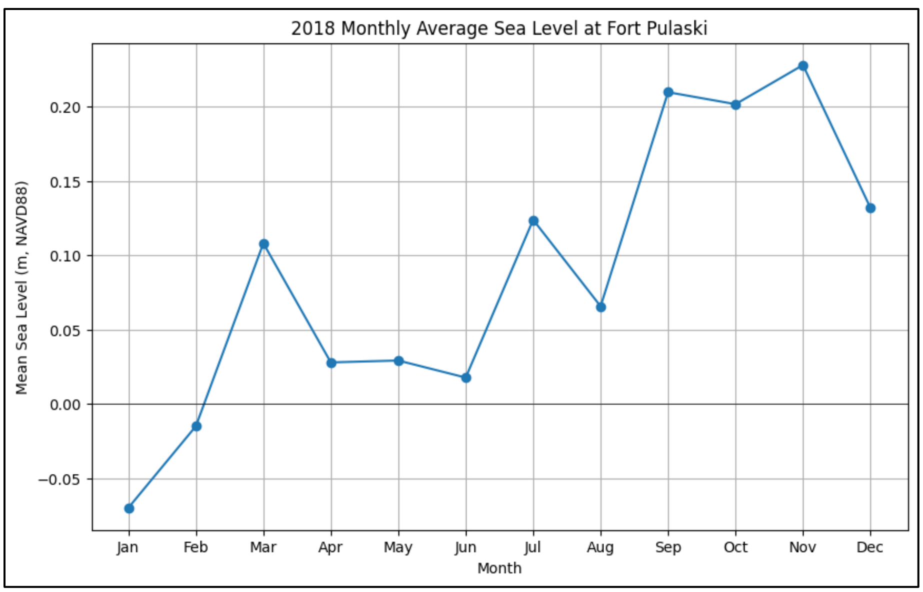

Figure 11 Monthly mean sea level (m) average for 2018. NOAA Fort Pulaski (8670870) station

3.2.3. Tides

The Savannah River mouth and outer navigation channel is characterized by strong tidal currents, which move water and sediment in and out of the system with the rise and fall of tides. The area exhibits a notable variation between neap tide currents and spring tide currents, which is consistent with typical tidal behaviors (Defne et al., 2011). Furthermore, in the continental shelf the direction of sediment movement is influenced by tidal flow, resulting in complex patterns of erosion and deposition. (Blanton et al., 2009).

Current wave dynamics analysis in the region shows that tidal forcing is a significant factor in the shelf region's hydrodynamics. The primary tidal force comes from the M2 tidal constituent, a regular cycle driven by the gravitational pull of the moon that repeats every 12 hours and 25 minutes, causing two high tides and two low tides daily (Blanton et al., 2003). Such tidal constituents dominate sea level and current tidal fluctuations. The cross-shelf variance is largely explained by semidiurnal tides, which contribute approximately 80% of the kinetic energy on the inner and middle shelf and around 30% on the outer shelf (Michel, 2013) (Edwards et al., 2006).

3.2.4. Waves

Wave characteristics described by Michel (2013) show that the monthly average wave heights on the outer shelf range from 1.5 to 2 meters, with mean wave periods of 4 to 6 seconds. The wave climate is relatively mild, except during the occurrence of hurricanes and tropical storms. It is characterized by the relative lack of frequent swell-period waves. The monthly variability in wave height is closely correlated with wind speeds, indicating that local winds are the primary driver of the wave climate in this region. Consequently, wave energy remains consistently lower in the southern part of the study area from January to September, while from October to December, wave heights are similar across offshore buoys of the Georgia coast.

The seasonal changes in winds, tides, and waves make the winter, spring, and summer-autumn periods the optimal time for analysis. The winter period (November to February) is characterized by the presence of strong southeasterly winds and intense tidal forces, which drive offshore currents and sediment transport. In spring (March–May), there is a shift in wind direction to the northeast, a weakening of tides, and a greater organization of wave patterns. Summer (June–July) and autumn (September–October) are characterized by southwestward winds that promote upwelling and along-shelf transport. August shares similar wind and wave conditions with July. Based on these distinct seasonal dynamics, the present analysis will be divided into four periods: winter, spring, and summer and autumn, including August within the summer period.

3.3 Hydrodynamic and Wave models

Simulations for the present research were performed in the ADvanced CIRCulation Model (ADCIRC) and the Simulating WAves Nearshore Model (SWAN). ADCIRC simulates water surface elevations, currents and depth-averaged velocities using the shallow water equations, wave continuity equations and depth-averaged momentum equations. (Luettich et al., 1992) (Luettich & Westerink, 2004) .SWAN solves the action balance equation for relative frequency and wave direction and simulates wind-generated waves (Booij et al., 1996) (Zijlema, 2010).

ADCIRC + SWAN simulations are coupled; ADCIRC provides water levels and depth-averaged currents to SWAN, which in turn calculates wave radiation stress gradients and feeds them back to ADCIRC (Bilskie et al., 2020). The two models are run in series on the same unstructured mesh. SWAN utilizes water levels and currents computed by ADCIRC, while ADCIRC is forced by radiation stress gradients calculated by SWAN. The models "leapfrog" through time, with ADCIRC executed first, followed by SWAN. This approach ensures efficient communication between models, using local memory without the need for costly global communication (Dietrich et al., 2012; Dietrich et al., 2011).

ADCIRC obtains water levels through solution of the Generalized Wave Continuity Equation (GWCE) (See Equation 13) (Luettich & Westerink, 2004) (Dietrich et al., 2011):

$$\frac{\partial^2 \zeta}{\partial t^2} + \tau_0 \frac{\partial \zeta}{\partial t} + \frac{\partial \widetilde{J_x}}{\partial x} + \frac{\partial \widetilde{J_y}}{\partial y} - UH \frac{\partial \tau_0}{\partial x} - VH \frac{\partial \tau_0}{\partial y} = 0 \tag{13}$$

where,

$$\begin{aligned} \widetilde{J_x} = -Q_x \frac{\partial U}{\partial x} - Q_y \frac{\partial U}{\partial y} + f Q_y - \frac{g}{2} \frac{\partial \zeta^2}{\partial x} - gH \frac{\partial}{\partial x}\left(\frac{P_s}{g\rho_0} - \alpha\eta\right) \\ + \frac{\tau_{sx,\mathrm{wind}} + \tau_{sx,\mathrm{waves}} - \tau_{bx}}{\rho_0} + M_x - D_x + U \frac{\partial \zeta}{\partial t} + \tau_0 Q_x \\ - gH \frac{\partial \zeta}{\partial x} \end{aligned} \tag{14}$$

$$\begin{aligned} \widetilde{J_y} = -Q_x \frac{\partial V}{\partial x} - Q_y \frac{\partial V}{\partial y} - f Q_x - \frac{g}{2} \frac{\partial \zeta^2}{\partial y} - gH \frac{\partial}{\partial y}\left(\frac{P_s}{g\rho_0} - \alpha\eta\right) \\ + \frac{\tau_{sy,\mathrm{wind}} + \tau_{sy,\mathrm{waves}} - \tau_{by}}{\rho_0} + M_y - D_y + V \frac{\partial \zeta}{\partial t} + \tau_0 Q_y \\ - gH \frac{\partial \zeta}{\partial y} \end{aligned} \tag{15}$$

Currents are obtained from the vertically-integrated momentum equations (equations 16 and 17):

$$\frac{\partial U}{\partial t} + U\frac{\partial U}{\partial x} + V\frac{\partial U}{\partial y} - fV = -g\frac{\partial \zeta}{\partial x} + \frac{P_s}{g\rho_0} - \alpha\eta + \frac{\tau_{sx,\mathrm{wind}} + \tau_{sx,\mathrm{waves}} - \tau_{bx}}{\rho_0 H} + \frac{M_x - D_x}{H} \qquad 16$$

and:

$$\frac{\partial V}{\partial t} + U\frac{\partial V}{\partial x} + V\frac{\partial V}{\partial y} + fU = -g\frac{\partial \zeta}{\partial y} + \frac{P_s}{g\rho_0} - \alpha\eta + \frac{\tau_{sy,\mathrm{wind}} + \tau_{sy,\mathrm{waves}} - \tau_{by}}{\rho_0 H} + \frac{M_y - D_y}{H} \qquad 17$$

where H=ζ+h is the total water depth; ζ is the deviation of the water surface from the mean; h is the bathymetric depth; U and V are depth integrated currents in the x-and y-directions, respectively; Q_x=UH and Q_y=VH are fluxes per unit width; f is the Coriolis parameter; g is the gravitational acceleration; P_s is the atmospheric pressure at the surface; ρ_0 is the reference density of water; η is the Newtonian equilibrium tidal potential and α is the effective earth elasticity factor; $\tau_{s,winds}$ and $\tau_{s,waves}$ are surface stresses due to winds and waves, respectively; τ_b is the bottom stress; M are lateral stress gradients; D are momentum dispersion terms; and τ_0 is a numerical parameter that optimizes the phase propagation properties.

The action balance equation is a governing equation (see Equation 18) of the SWAN model. It describes the transport of wave action density in both geographical and spectral space, considering various physical processes such as wave propagation, refraction, diffraction, wind growth, wave breaking, and bottom friction (Booij et al., 1999a);

$$\frac{\partial N}{\partial t} + \nabla_{\vec{x}} \cdot (\overrightarrow{c_g} + \vec{U})N + \frac{\partial c_\theta N}{\partial \theta} + \frac{\partial c_\sigma N}{\partial \sigma} = \frac{S_{tot}}{\sigma} \qquad 18$$

where, σ= the relative frequency and θ= the wave direction.

3.3.1. Model Setup

An unstructured finite element mesh was utilized within the Western North Atlantic Tidal (WNAT) domain, encompassing the intertidal zones of the South Atlantic Bight (SAB) estuaries (Hagen et al., 2006) (Bacopoulos et al., 2011). The mesh exhibited a gradient in resolution, increasing as it approached the shoreline; the grid resolution was refined within the Savannah Harbor navigation channel, where a 1-meter resolution digital elevation model (DEM) obtained from the Topographic Information for the Nation by the USGS (2019) was interpolated to enhance the elevation accuracy in that section. The final mesh comprised 1,008,384 elements and 541,906 nodes. WNAT domain and increased bathymetry resolution in the Savannah Harbor navigation channel is shown in Figure 12 and Figure 13.

Seven astronomic tidal constituents were included in tidal forcing of the open-ocean boundary (O_1, K_1, Q_1, M_2, N_2, S_2, and K_2) (Hagen et al., 2006).

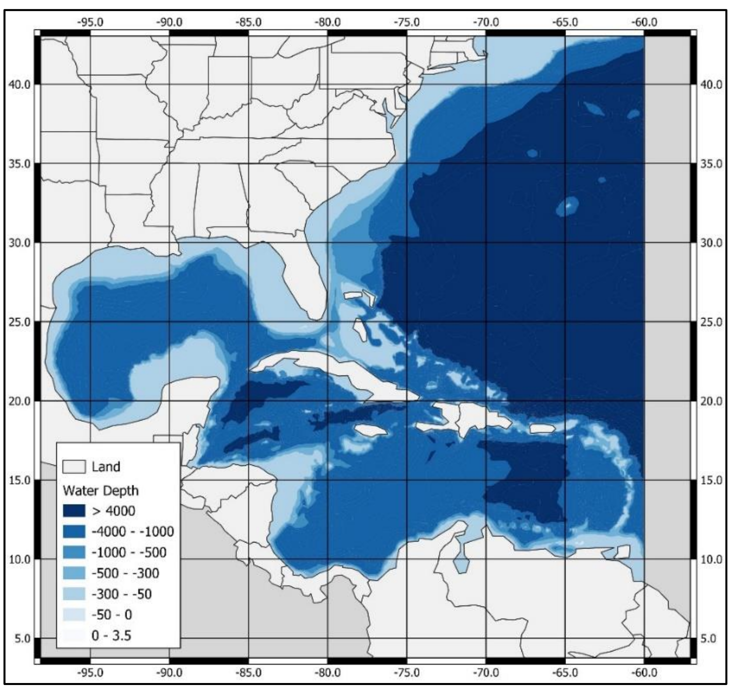

Figure 12 WNAT model domain

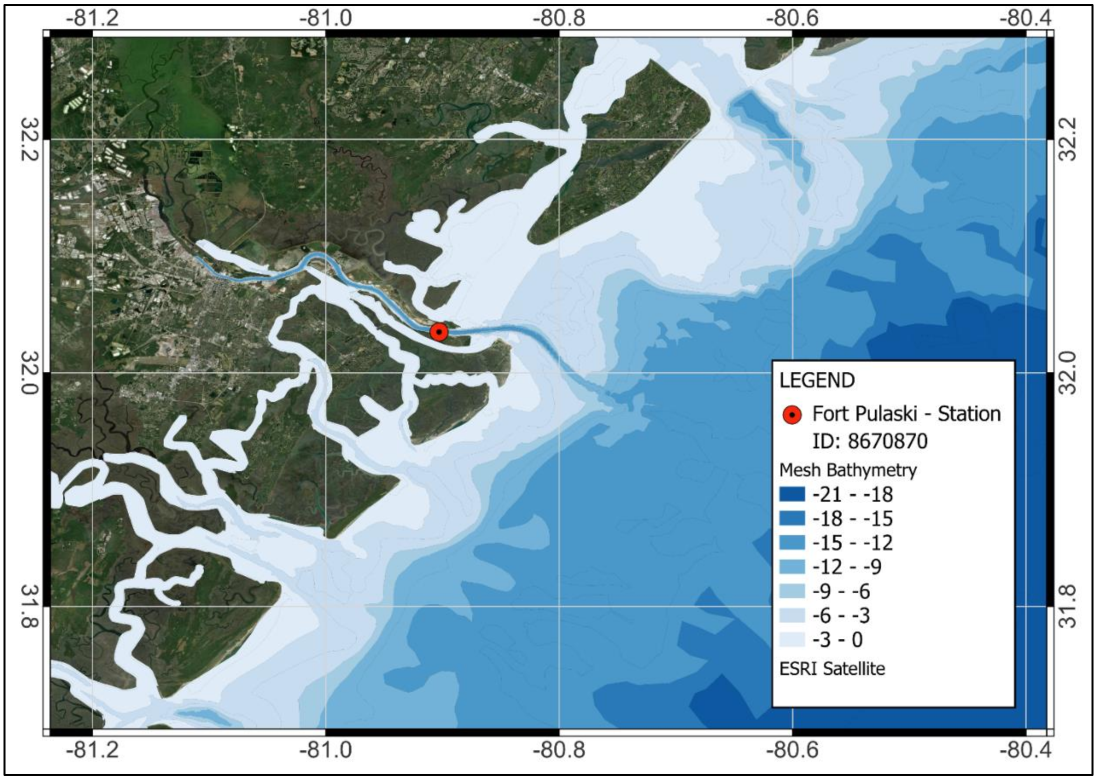

Figure 13 Mesh Bathymetry

The 10-meter u-component of wind and the 10-meter v-component of wind, as well as the mean sea level pressure values, were obtained from the ERA5 dataset provided by the European Centre for Medium-Range Weather Forecasts (ECMWF) (Hersbach et al., 2020) (ECMWF, 2024). The ERA5 data was retrieved in NetCDF format and subsequently processed using a MATLAB script before being exported to meteorological (wind and pressure) input files.

The coupled ADCIRC-SWAN simulation was configured to generate spectral files for specific locations within the study area (Delft, 2024). The simulation yielded detailed wave energy distributions over frequency and direction.

The results obtained from the simulations, including water surface elevation, wave height and wave energy spectrum, were plotted monthly. These results were then analyzed over four different periods: winter, spring, summer and autumn, as described in section 3.2. Winds, Tides and Waves.

3.3.2. Hydrodynamics and Wave Results Comparison

The water surface elevation results from the hydrodynamic run were compared with measurements taken by NOAA at Fort Pulaski, GA, Station ID: 8670870. The significant wave height results obtained from the spectral wave simulation were validated against data from two NOAA National Data Buoy Center stations. These stations include Station 41008 (LLNR 833) located at Grays Reef, 40 nautical miles southeast of Savannah, GA, and Station 41112, positioned offshore near Fernandina Beach, FL (Figure 14).

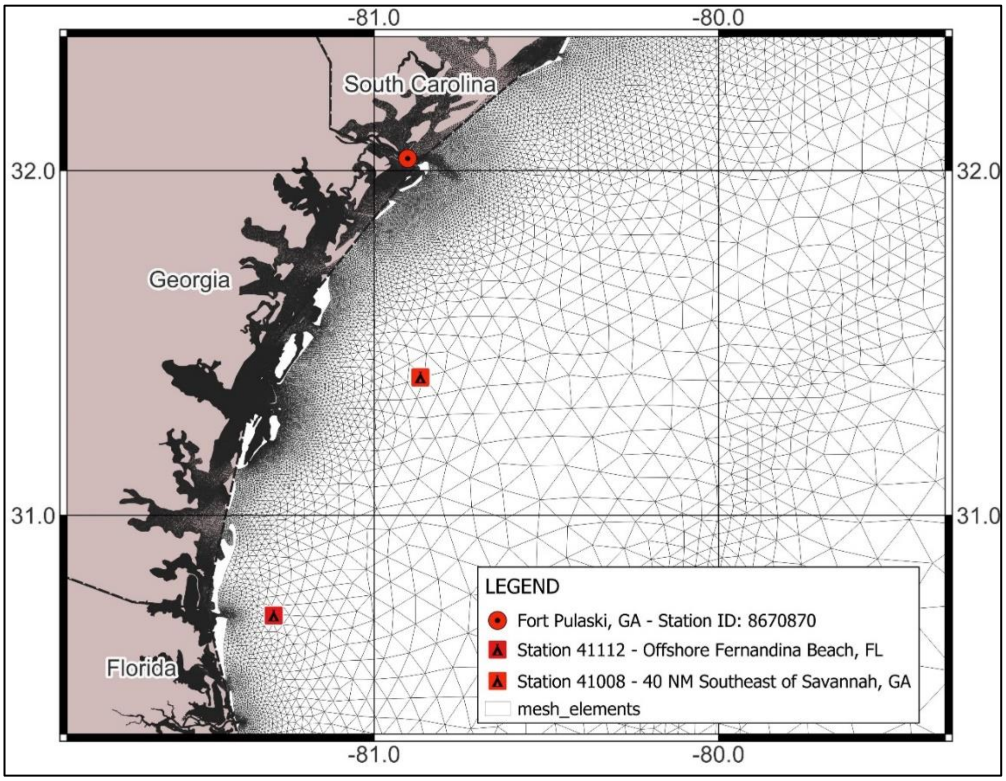

Figure 14 NOAA stations and buoys.

3.4. Energy Spectrum

Energy spectrum plots were made at five locations in and around the Savannah River Channel. One point was located at the mouth of the river, while two other points were located in the outer channel east of Tybee Island. A fourth point was located in the north channel. Two additional points were selected outside the immediate study area: one near Pritchards Island, South Carolina, and another near Little St. Simons Island, Georgia. (see Figure 15).

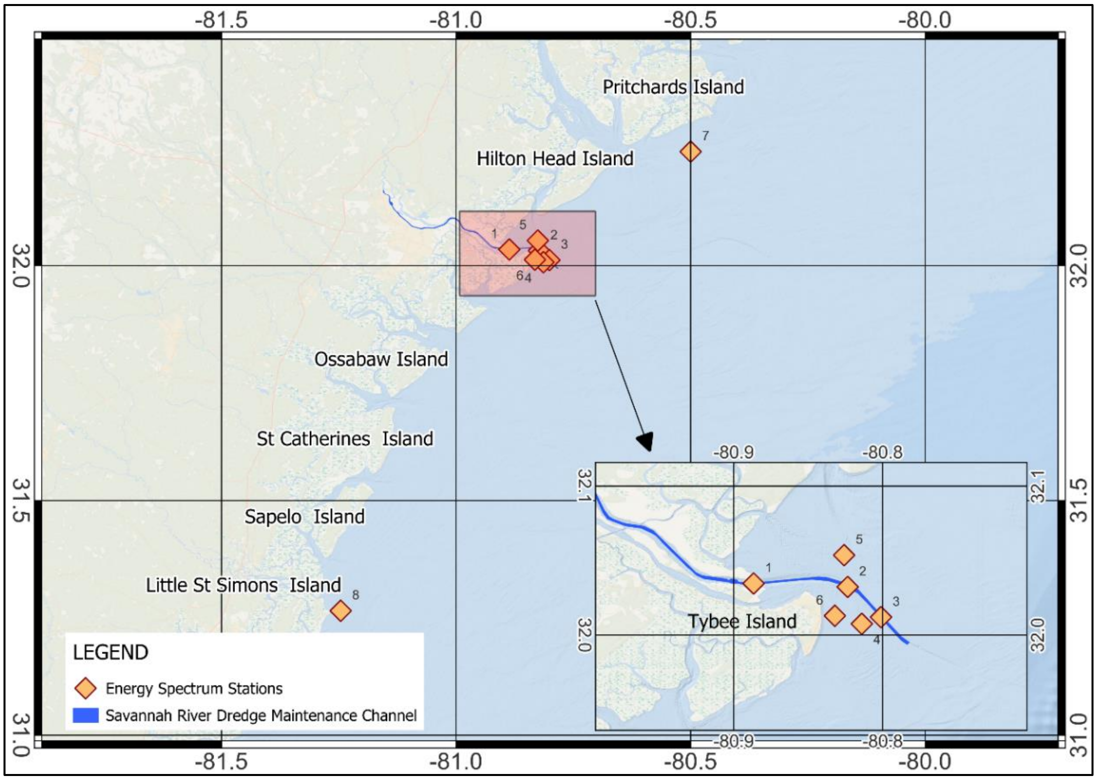

Figure 15 Location of Spectrum Energy Charts were generates

For the present analysis, the focus was on four stations: the river mouth (Station 1), east of Tybee Island (Station 6), the outer channel (Station 3), and near St. Simons Island (Station 8). These stations were chosen to provide a representative overview of the wave energy spectrum across key areas of interest.

3.5. Sediment characteristics

Data from several sediment surveys were compiled. These surveys include those conducted by the U.S. Geological Survey (USGS) for the USSEABED project in 2004, as well as the U.S. Army Corps of Engineers, Savannah District in 2002 (USACE, 2002b). Additional data was gathered from the Skidaway Institute of Oceanography in the years 1994, 1995, 2000, 2001, 2014, and 2020 (SKIO, 2022). A total of 527 sediment samples were included in the study.

These samples were primarily located in the navigation channel but also included other locations close to the shore. The results of the sediment size analysis were used to determine the grading coefficient in the sediment model. Figure 16 shows the location of the different sediment samples.

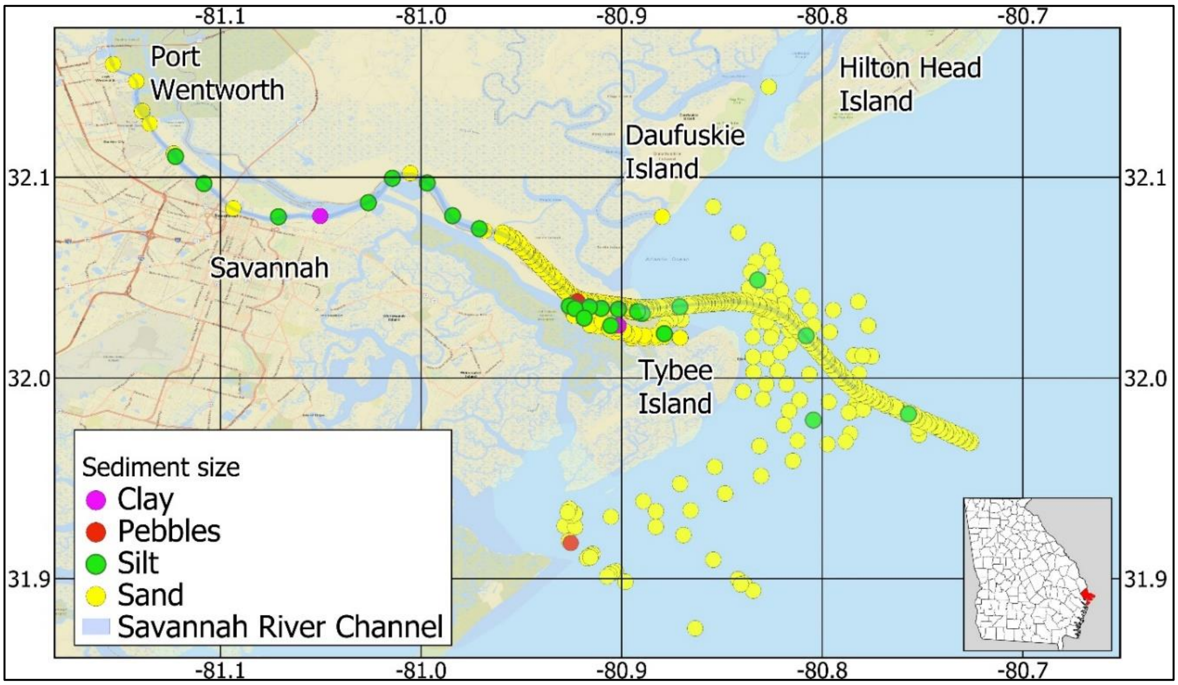

Figure 16 Sediment size samples in the study area

As shown in Figure 16, the sediment is predominantly sandy, with a notable proportion of medium to coarse sand. Fine sediments such as clay and silt are minimal, suggesting that the sediment transport environment is likely influenced by relatively high-energy conditions, which favor the deposition of larger particles. The small percentages of very coarse sand and pebbles indicate stronger current flows in inlets along the coast.

Figure 17 provides closer illustration of the sediment size observed in the Savannah Harbor sections where littoral transport is active. Sandy composition was observed in the outer channel as well as in some sections in the inner channel, which indicates that sediment transported by longshore transport processes is transported to some of the sections in the inner channel (Olsen Associates, 2002).

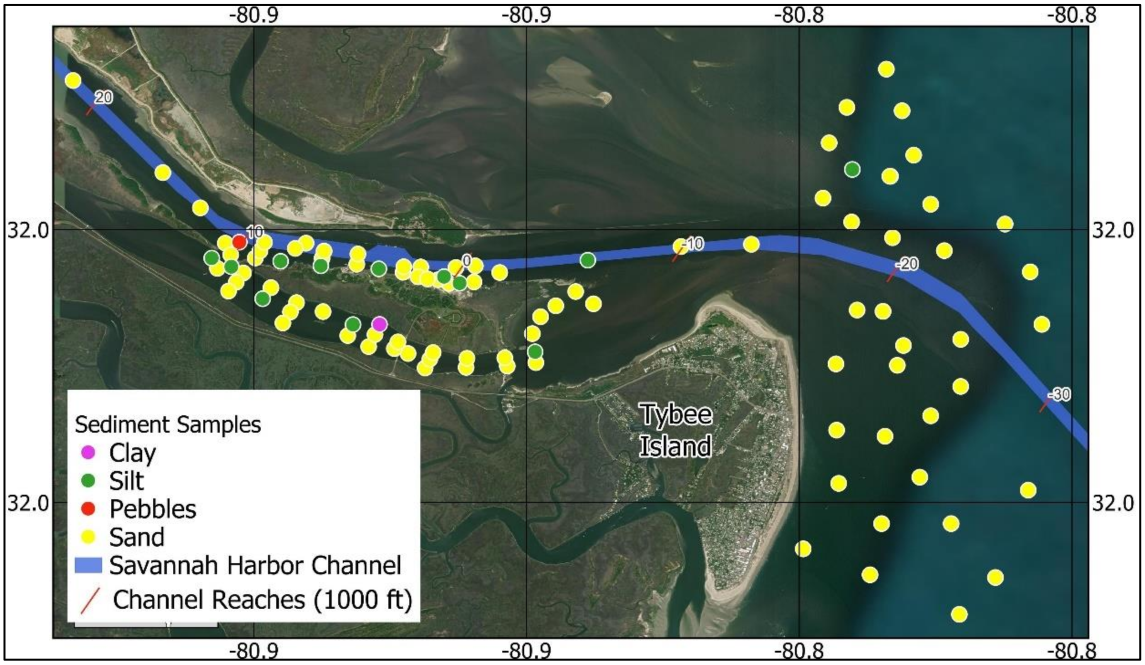

Figure 17 Sediment size in sections where littoral transport occurs

3.6 Savannah Harbor Navigation Channel Dredging Records

Daily dredging records from 2013 to 2022 were provided by the USACE Savannah District used for the present analysis. These records detail the specific reach sections where dredging occurred. Reaches are 10,000-foot-long segments, distributed evenly along the primary federal channel line, maintaining the reach numeration used by the USACE

Dredging records for the outer channel did not include new work dredging associated with the SHEP new work, which took place from 2015 to 2018. Consequently, LST based on dredging data for the outer channel was estimated by using only maintenance dredging volumes.

Annual maintenance dredging for the inner channel were obtained from Sytsma C. et al. (2023) calculated as the average volume dredged from 2013 to 2018.

This methodology enabled the calculation of the total dredged volumes for each reach section (Figure 18).

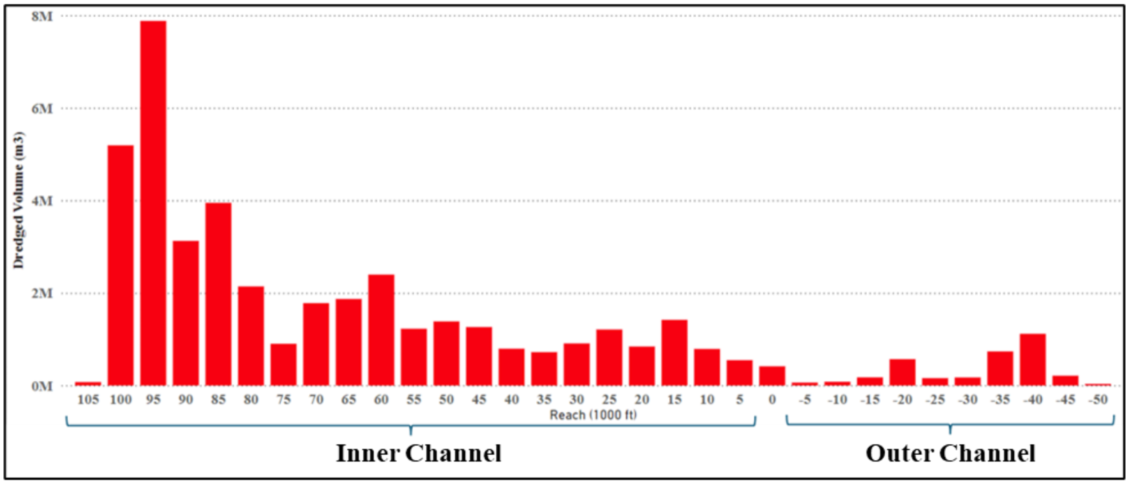

Figure 18 Total dredged volumes along the navigation channel reaches

The total annual volume of maintenance dredging for the inner and outer harbors is illustrated in Figure 19 and Figure 20. From 2013 to 2022, the average annual volume of 2,514,906 m³/year of material was dredged from the inner channel, while 432,052 m³/year of sediment was dredged from the outer channel to maintain the authorized depth.

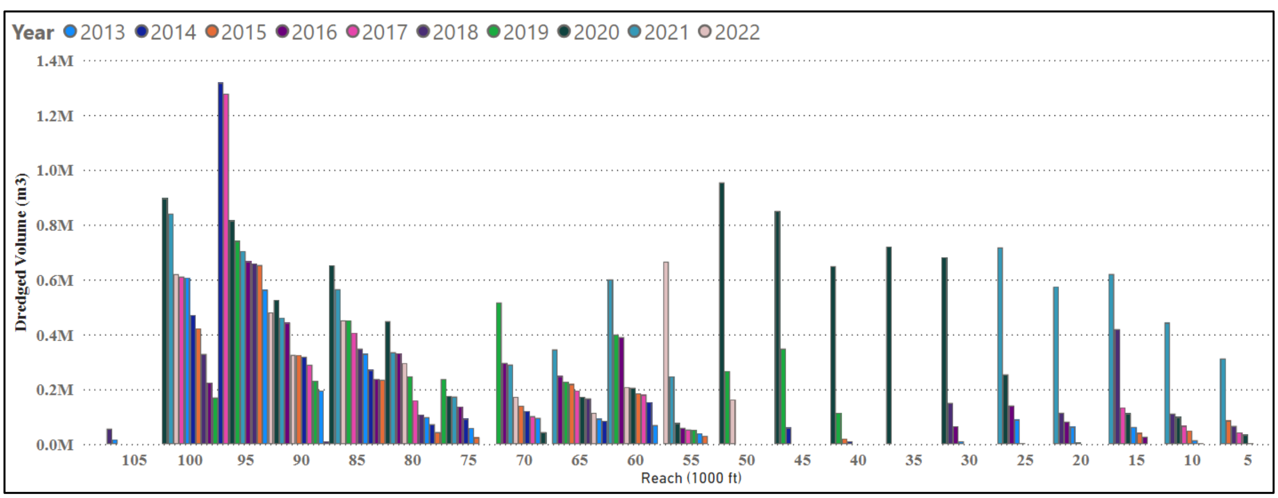

Figure 19 Dredging volumes in the inner channel

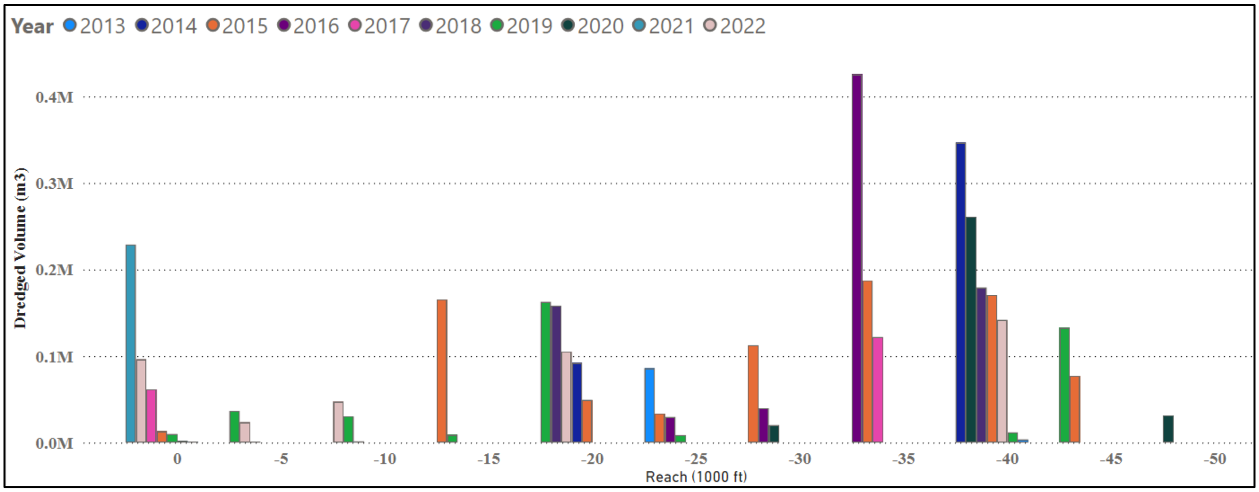

Figure 20 Dredging volumes in the outer channel

Sediment sources for the outer channel include longshore transport from the north, which is equals to beach sediments along Tybee Island, Turtle Island, Daufuskie Island, and Barrett Shoals (Olsen Associates, 2002; Smith et al., 2008). Given the sediment size analysis shown in section 3.5. Sediment characteristics, the LST can be estimated from the maintenance dredging volumes for the outer harbor and the inner channel in sections 0+000 to 24+000.

3.7 Longshore sediment transport using CERC (1984) equation

LST was estimated at three points near Tybee Island: one to the north, one to the east, and one to the southeast of the island. Wave simulation results were used to compute LST based on the CERC (1984) equation. These selected points lie within the breaking area. This zone is characterized by active sediment transport driven by wave breaking and nearshore currents (Reeve et al., 2018).

3.8. River inputs

The sediment input values for the Savannah River utilized in the present analysis were derived from Sytsma C. et al. (2023). The authors employed a two-bin method to calculate daily loads from available discharge data spanning from 1974 to the present. Median sediment concentrations were aggregated to determine annual loads, with the average annual load based on the most recent 20 years. This analysis yielded an estimated annual average sediment load of 146,000 m^3/year.

CHAPTER 4 RESULTS

4.1. Hydrodynamic and wave modeling

The statistical results for the hydrodynamic run of water surface elevation at Fort Pulaski provide insight into the accuracy and performance of the model in comparison to the measured data across a period of several months (Table 1). The analysis uses Root Mean Square Error (RMSE), mean bias (MN Bias), Scatter Index, and Nash–Sutcliffe model efficiency coefficient (NSE) to assess model performance.

In late winter (Jan–Feb), RMSE was 0.189 m, and mean bias was -0.101 m, indicating an underestimation of water surface elevation. The Scatter Index, at 0.261, shows moderate variability relative to observed data, while the Nash-Sutcliffe Efficiency (NSE) of 0.939 reflects close alignment with observed values. In spring (Mar–May), RMSE increased to 0.269 m, and mean bias decreased to -0.215 m, indicating a greater degree of underestimation. The Scatter Index rose to 0.323, and NSE declined to 0.884, suggesting increased error variability in the spring period.

During summer (Jun–Aug), RMSE reached 0.274 m, with mean bias further decreasing to -0.270 m, reflecting underestimation. The Scatter Index of 0.284 was slightly lower than in spring, and NSE remained stable at 0.881. In autumn (Sep–Oct), RMSE increased to 0.389 m, and mean bias shifted to -0.467 m, marking the highest underestimation among all periods. The Scatter Index rose to 0.329, and NSE dropped to 0.735, indicating an increase in error variability during autumn.

For early winter (Nov–Dec), RMSE remained at 0.388 m, with mean bias at -0.417 m and a Scatter Index of 0.364. The NSE, at 0.757, suggests some recovery in alignment with observed values compared to autumn, though with persistent underestimation.

In the annual summary (Jan–Dec), RMSE was calculated at 0.233 m, with a mean bias of -0.230 m, demonstrating underestimation across the year. The Scatter Index of 0.246 reflects stable error variability throughout the period, while NSE at 0.912 indicates alignment with observed data across all time periods.

Table 1 Statistical Performance of Hydrodynamic Model for Fort Pulaski Across Simulation Periods - water surface elevation

Simulation Period	RMSE (m)	MN Bias (m)	Scatter Index	NSE
Jan – Feb (late winter)	0.189	-0.101	0.261	0.939
Mar – May (spring)	0.269	-0.215	0.323	0.884
Jun – Aug (summer)	0.274	-0.270	0.284	0.881
Sep – Oct (autumn)	0.389	-0.467	0.329	0.735
Nov – Dec (early winter)	0.388	-0.417	0.364	0.757
Overall (Jan-Dec)	0.233	-0.230	0.246	0.912

Monthly observed vs hindcast water surface elevation in Fort Pulaski, are shown in Figure 21 to Figure 32:

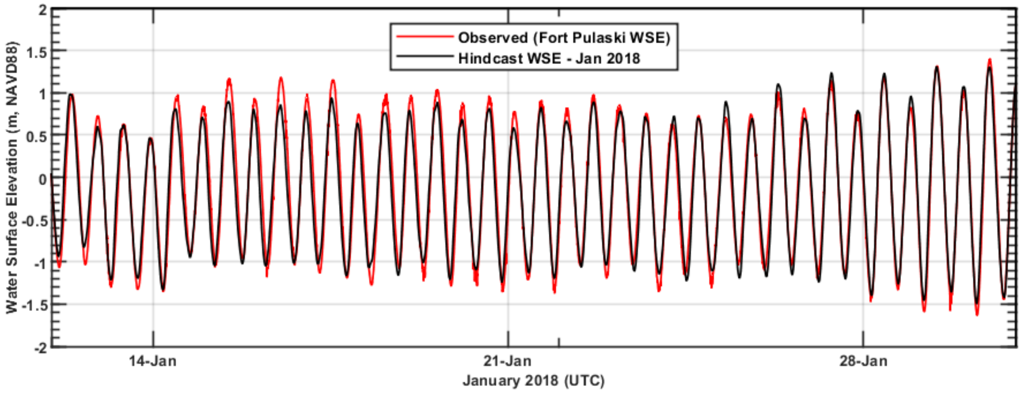

Figure 21 Fort Pulaski Observed vs hindcast water surface elevation – January 2018

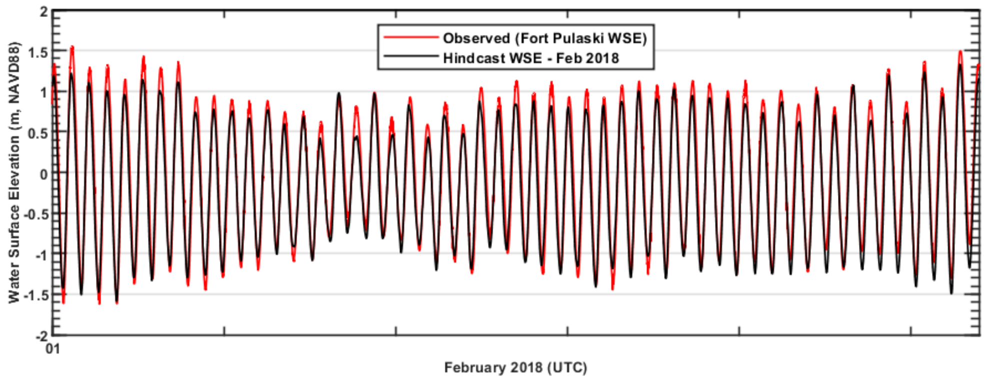

Figure 22 Fort Pulaski Observed vs hindcast water surface elevation – February 2018

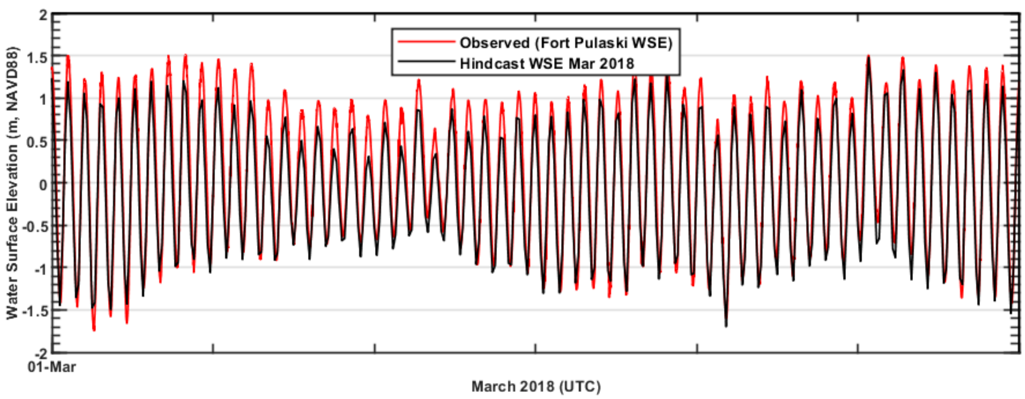

Figure 23 Fort Pulaski Observed vs hindcast water surface elevation – March 2018

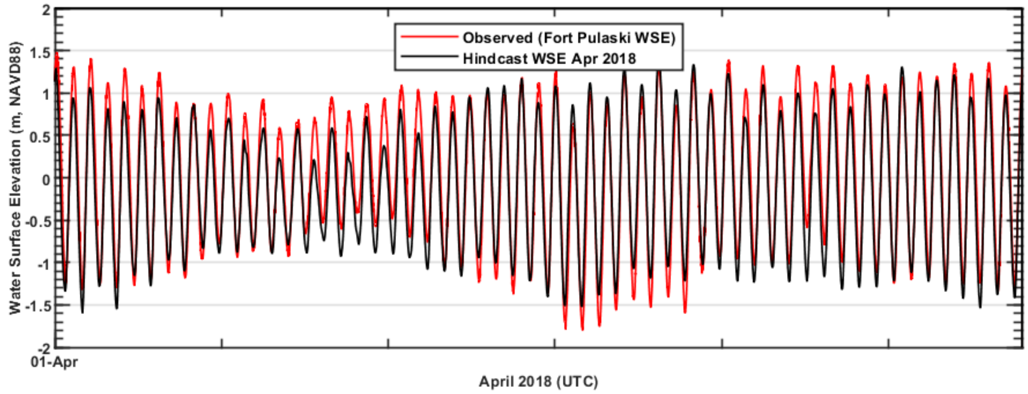

Figure 24 Fort Pulaski Observed vs hindcast water surface elevation – April 2018

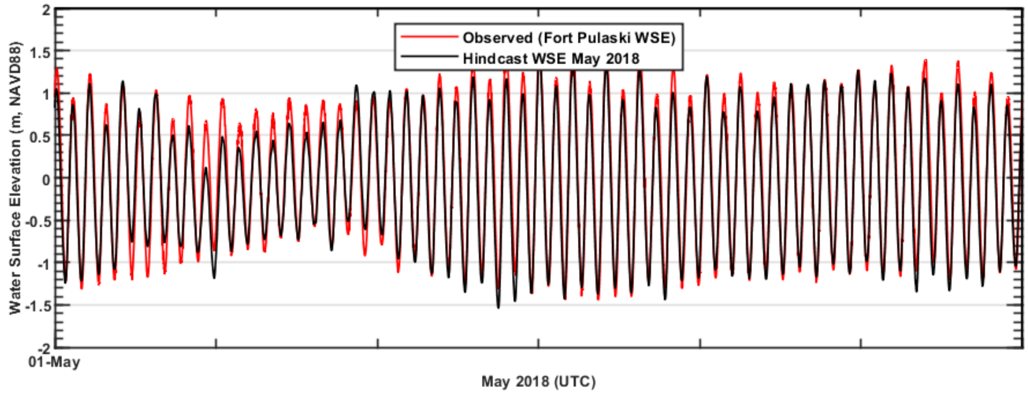

Figure 25 Fort Pulaski Observed vs hindcast water surface elevation – May 2018

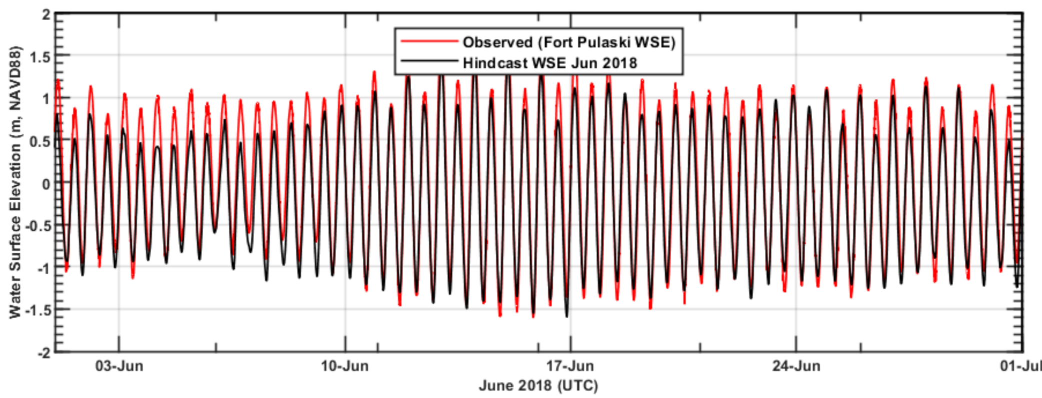

Figure 26 Fort Pulaski Observed vs hindcast water surface elevation – Jun 2018

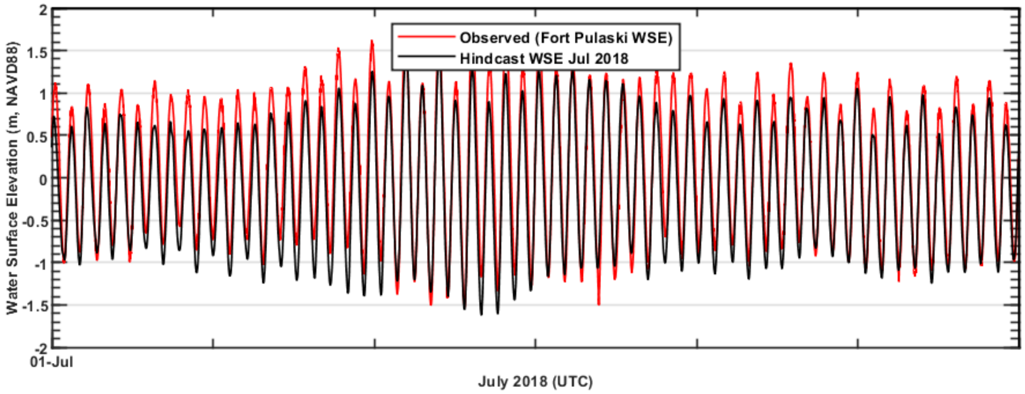

Figure 27 Fort Pulaski Observed vs hindcast water surface elevation – Jul 2018

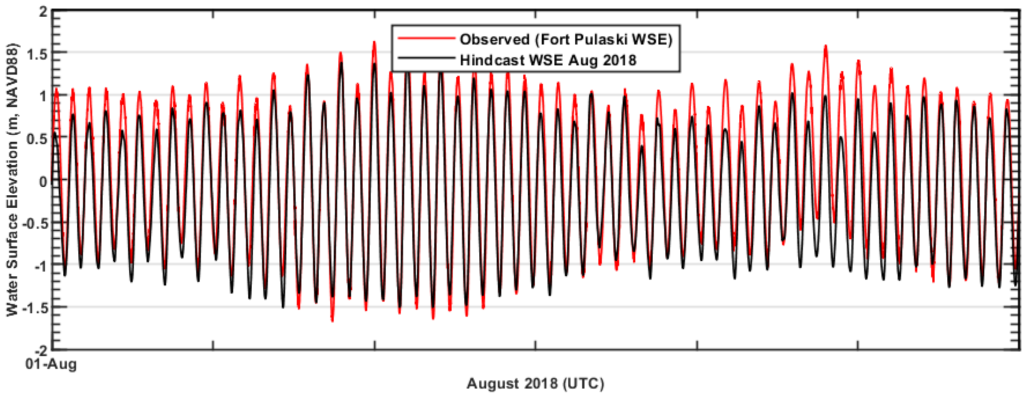

Figure 28 Fort Pulaski Observed vs hindcast water surface elevation – Aug 2018

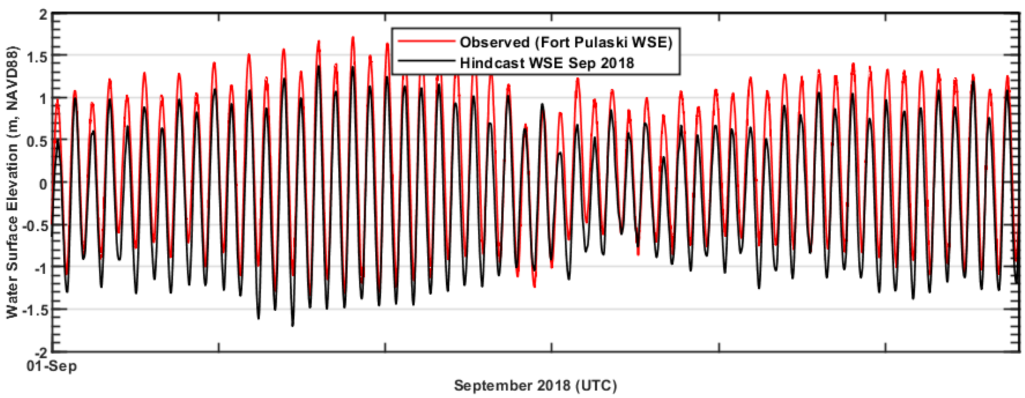

Figure 29 Fort Pulaski Observed vs hindcast water surface elevation – Sep 2018

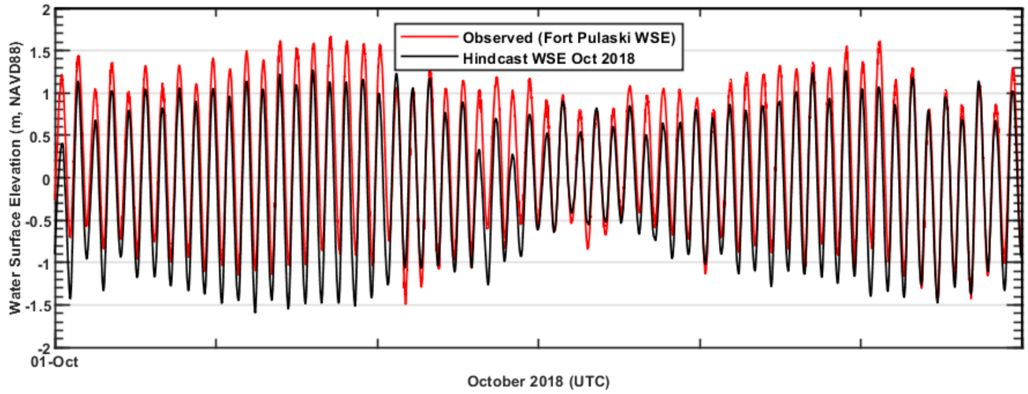

Figure 30 Fort Pulaski Observed vs hindcast water surface elevation – Oct 2018

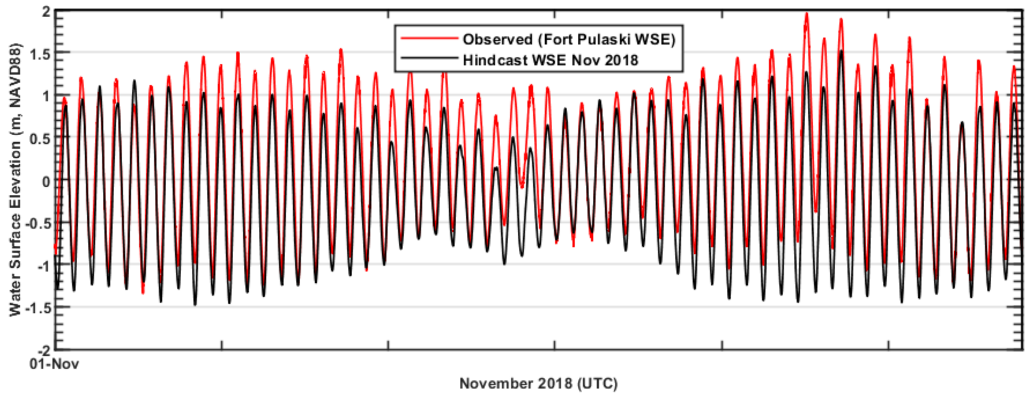

Figure 31 Fort Pulaski Observed vs hindcast water surface elevation – Nov 2018

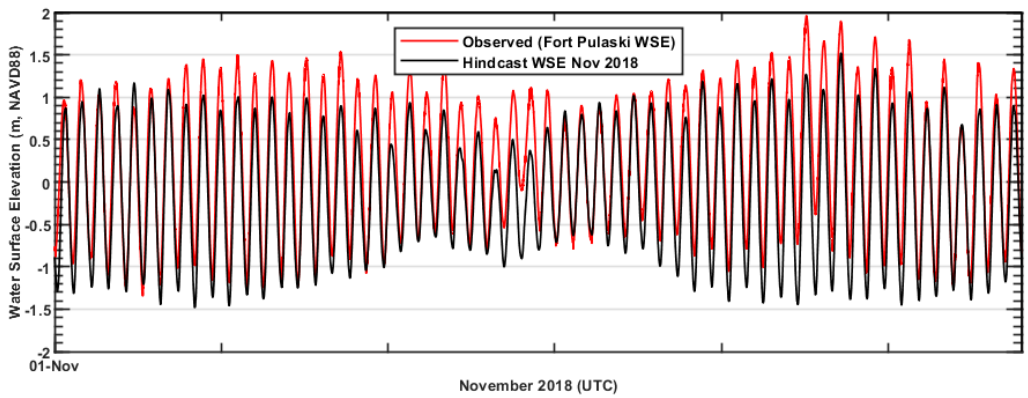

Figure 32 Fort Pulaski Observed vs hindcast water surface elevation – Dic 2018

Table 2 presents the statistical performance metrics—Root Mean Square Error (RMSE), mean bias (MN Bias), Scatter Index and Nash-Sutcliffe Efficiency index—of the SWAN wave model simulation for significant wave height at buoys 41008 and 41112 over the established analysis periods throughout the year.

Table 2 Statistical Performance of Wave Model for Buoys 41008 and 41112 Across Simulation Periods- significant wave height (Hs)

	Buoy 41008				**Buoy 41112**			
Simulation Period	RMSE (m)	MN Bias (m)	Scatter Index	NSE	RMSE (m)	MN Bias (m)	Scatter Index	NSE
Jan – Feb (late winter)	0.217	0.105	0.189	0.646	0.181	0.102	0.162	0.716
Mar – May (spring)	0.223	0.107	0.188	0.696	0.236	0.100	0.228	0.648
Jun – Aug (summer)	0.122	0.069	0.162	0.715	0.103	0.036	0.165	0.720
Sep – Oct (autumn)	0.255	0.007	0.247	0.629	0.248	-0.016	0.252	0.632
Nov – Dec (early winter)	0.278	0.081	0.243	0.724	0.251	0.051	0.253	0.711
Overall (Jan-Dec)	0.218	0.074	0.218	0.731	0.207	0.056	0.232	0.725

At buoy 41112, the model produced an RMSE of 0.181 m and a mean bias of 0.102 m in late winter (Jan–Feb), indicating a slight overestimation. The Scatter Index was 0.162, with an NSE of 0.716, reflecting consistent alignment with observed values. Spring (Mar–May) exhibited an increased RMSE of 0.236 m and a Scatter Index of 0.228 m, with an NSE of 0.648, indicating greater error variability. Summer (Jun–Aug) yielded the lowest RMSE (0.103 m) and mean bias (0.036 m), with an NSE of 0.720, marking this period as having the least error magnitude.

Autumn (Sep–Oct) displayed an RMSE of 0.248 m, with a mean bias of -0.016 m, showing slight underestimation and increased variability (Scatter Index of 0.252), with NSE at 0.632. Early winter (Nov–Dec) results were similar, with an RMSE of 0.251 m and an NSE of 0.711, indicating slight improvement over autumn.

The annual result (Jan–Dec) showed an RMSE of 0.207 m and mean bias of 0.056 m, with a Scatter Index of 0.232 and the highest NSE (0.725) for the entire period, reflecting consistent performance across all seasonal divisions.

Model errors were lowest in summer and highest in autumn, with the annual summary indicating stability in reproducing observed wave height across time intervals. Observed vs hindcast results of significant wave height for buoy 41112 is shown in Figure 33 to Figure 37:

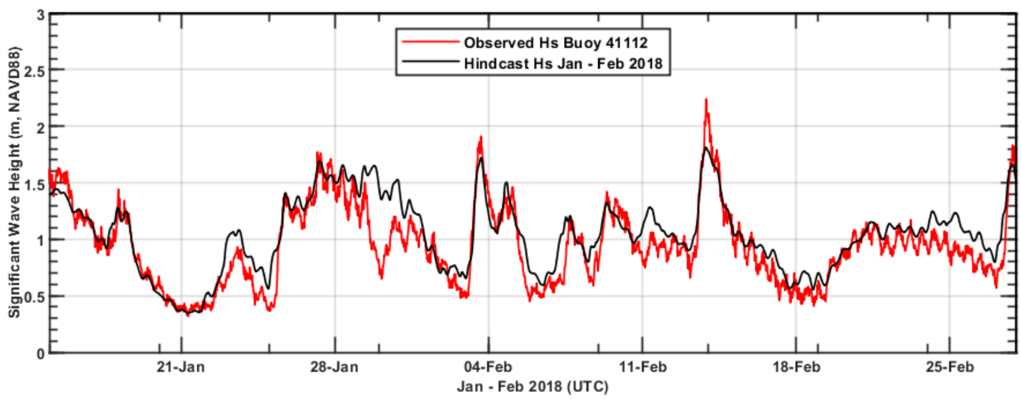

Figure 33 Buoy 41112 Observed vs hindcast significant wave height Jan-Feb 2018

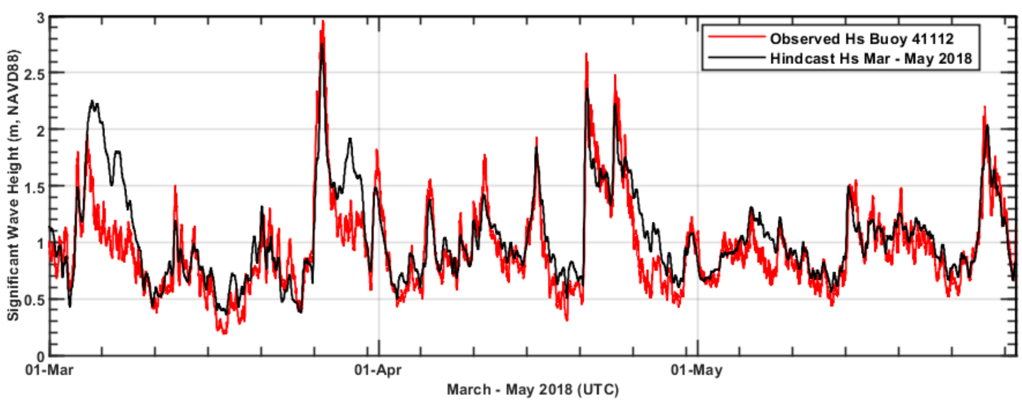

Figure 34 Buoy 41112 Observed vs hindcast significant wave height Mar-May 2018

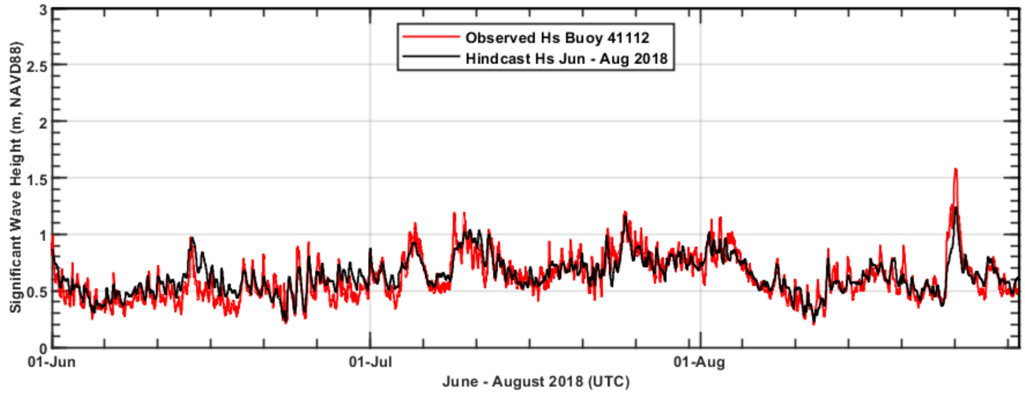

Figure 35 Buoy 41112 Observed vs hindcast significant wave height Jun-Aug 2018

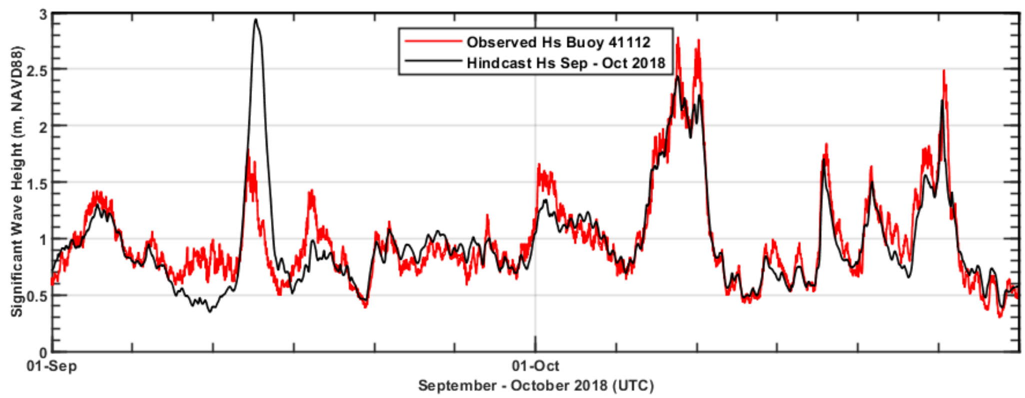

Figure 36 Buoy 41112 Observed vs hindcast significant wave height Sep-Oct 2018

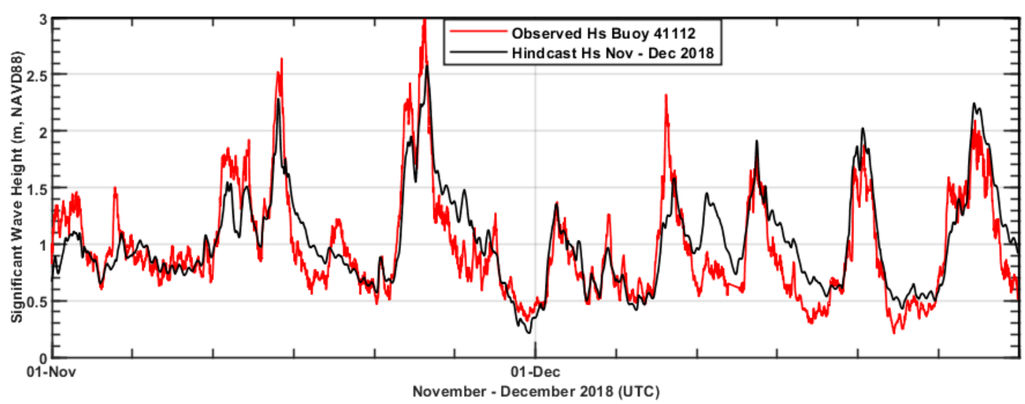

Figure 37 Buoy 41112 Observed vs hindcast significant wave height Nov-Dic 2018

For buoy 41008, in late winter (Jan–Feb), the model produced an RMSE of 0.217 m and a mean bias of 0.105 m, suggesting a slight overestimation of wave heights. The Scatter Index was 0.189, and the Nash-Sutcliffe Efficiency (NSE) was 0.646, indicating moderate alignment with observations. During spring (Mar–May), RMSE decreased slightly to 0.223 m, mean bias rose to 0.107 m, and NSE improved to 0.696, suggesting a modest increase in performance stability over the previous season.

The summer period (Jun–Aug) exhibited the lowest RMSE (0.122 m) and mean bias (0.069 m), accompanied by a Scatter Index of 0.162, indicating reduced error and variability. The NSE for summer was 0.715, representing the highest seasonal fit.

In autumn (Sep–Oct), the model showed an RMSE of 0.255 m and a near-zero mean bias of 0.007 m, with a Scatter Index of 0.247 and NSE dropping to 0.629, indicating increased variability.

Early winter (Nov–Dec) had the highest RMSE (0.278 m) and mean bias (0.081 m) of the periods, with a Scatter Index of 0.243. Despite the increase in error, the NSE reached 0.724, demonstrating a relatively stable performance.

The overall annual analysis (Jan–Dec) yielded an RMSE of 0.218 m and mean bias of 0.074 m, with a Scatter Index of 0.218 and the highest NSE (0.731), reflecting consistent alignment between model and observed data. Overall, model accuracy was highest in summer and early winter, with variability peaking in autumn and remaining consistent throughout the annual summary. Wave modeling results comparison with NOAA buoy 41008 area shown in Figure 38 to Figure 42.

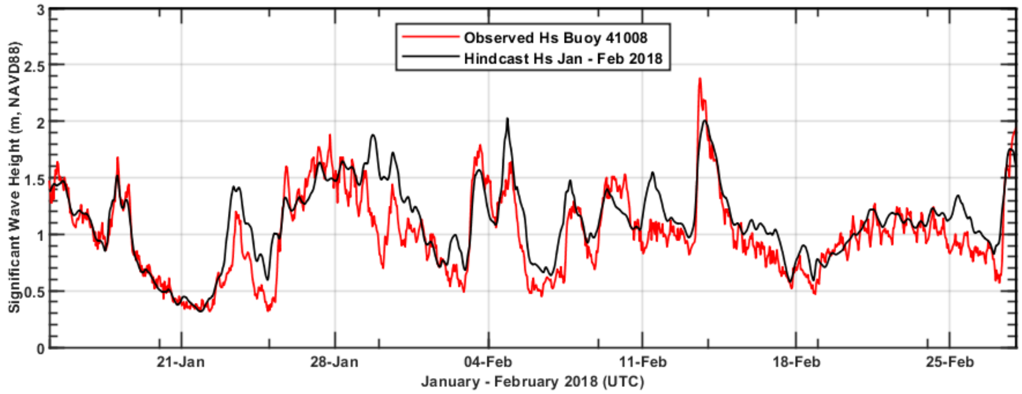

Figure 38 Buoy 41008 Observed vs hindcast significant wave height Jan-Feb 2018

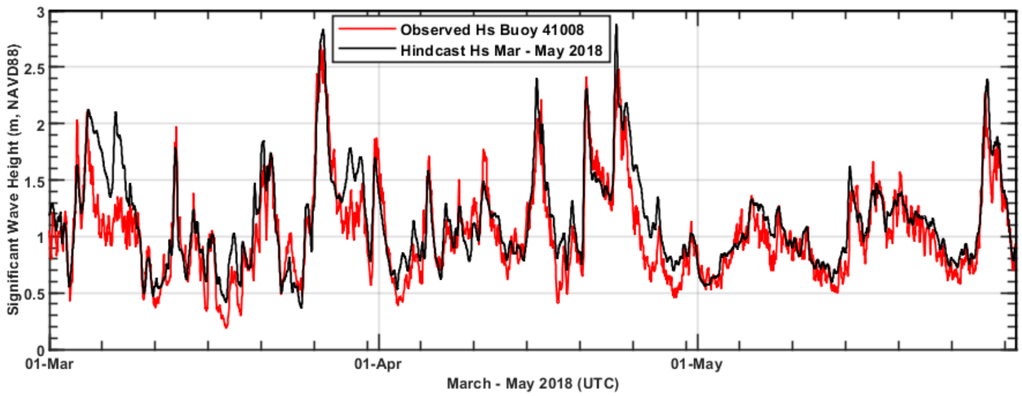

Figure 39 Buoy 41008 Observed vs hindcast significant wave height Mar-May 2018

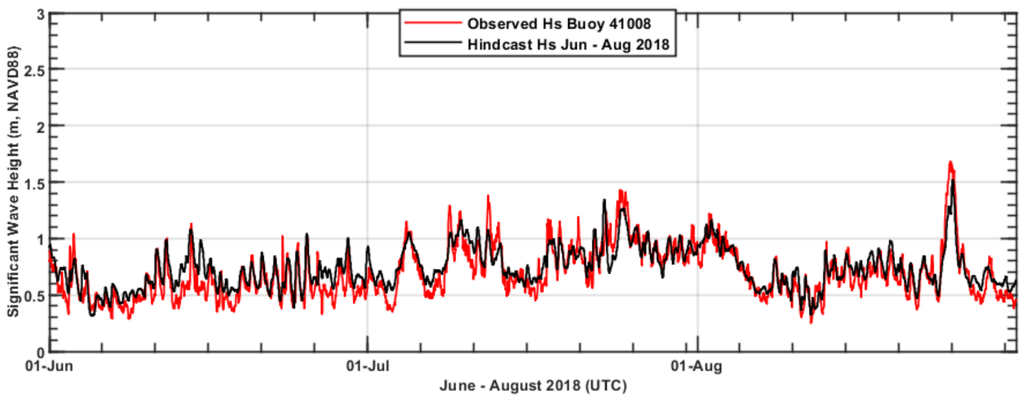

Figure 40 Buoy 41008 Observed vs hindcast significant wave height Jun-Aug 2018

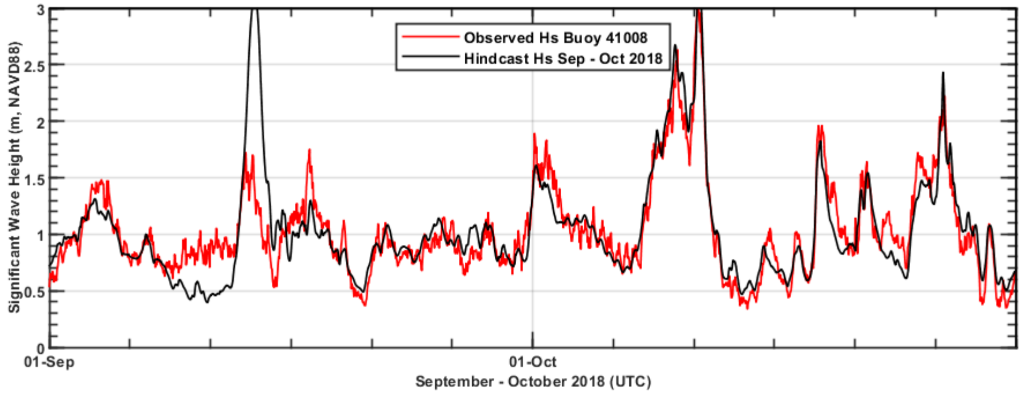

Figure 41 Buoy 41008 Observed vs hindcast significant wave height Sep-Oct 2018

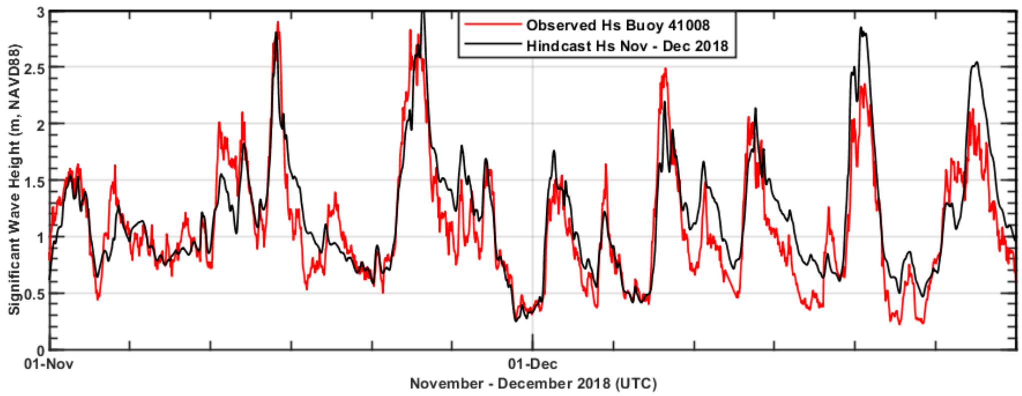

Figure 42 Buoy 41008 Observed vs hindcast significant wave height Nov-Dic 2018

4.2. Energy spectrum

Figure 43 shows the energy spectra in the January-February period at the four stations. The energy spectrum for Station 6 and Station 3 shows a broad distribution, with the highest energy (highlighted in white) predominantly directed to the north and northwest. In contrast, Station 1, located at the mouth of the river, has a more concentrated energy distribution oriented towards the north. Meanwhile, Station 8, located south of the study area, indicates a northward flow of energy during this time of year.

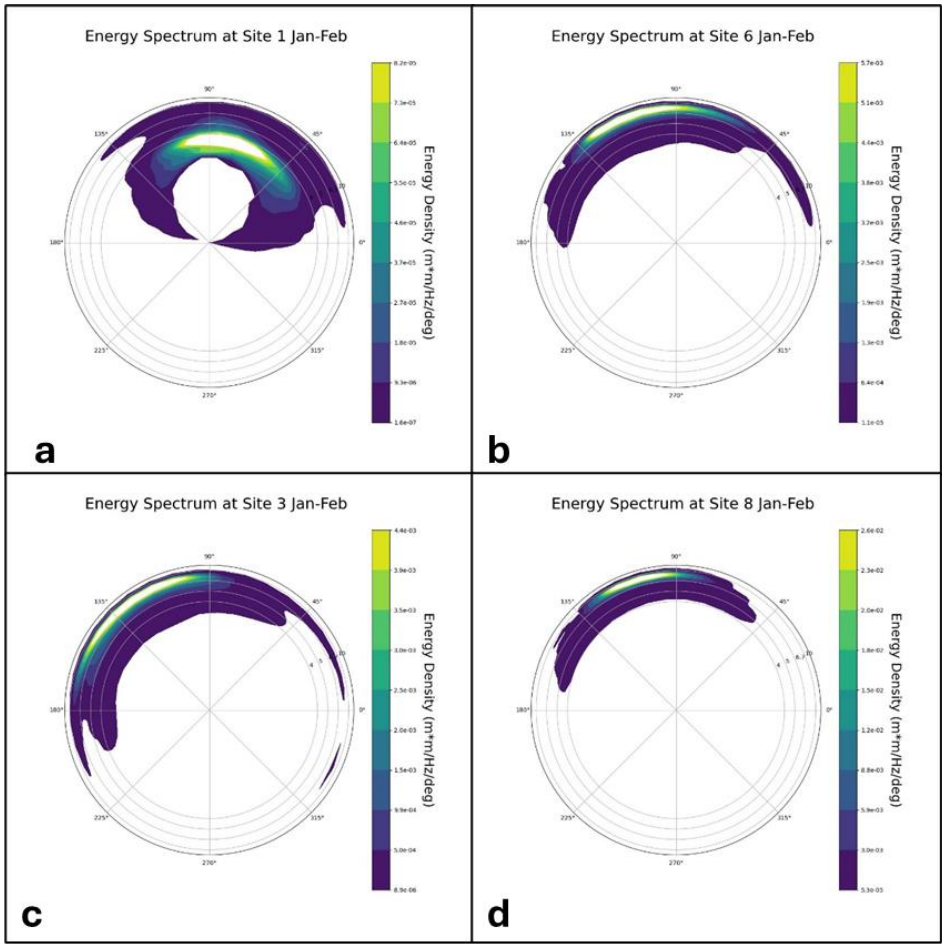

Figure 43 Energy Spectrum During Late Winter
(a) Station 1, (b) Station 6, (c) Station 3, (d) Station 8

Figure 44 shows the energy spectra in the spring period at the four stations. Station 6, located east of Tybee Island, and Station 3, located in the outer channel, exhibit a broad energy spectrum distribution from west to north. In contrast, Station 1, located at the mouth of the river, shows a more focused energy distribution concentrated to the north and southwest, with comparatively lower energy density values. Station 8, located south of the study area, has a broad distribution with the highest energy concentrated to the north.

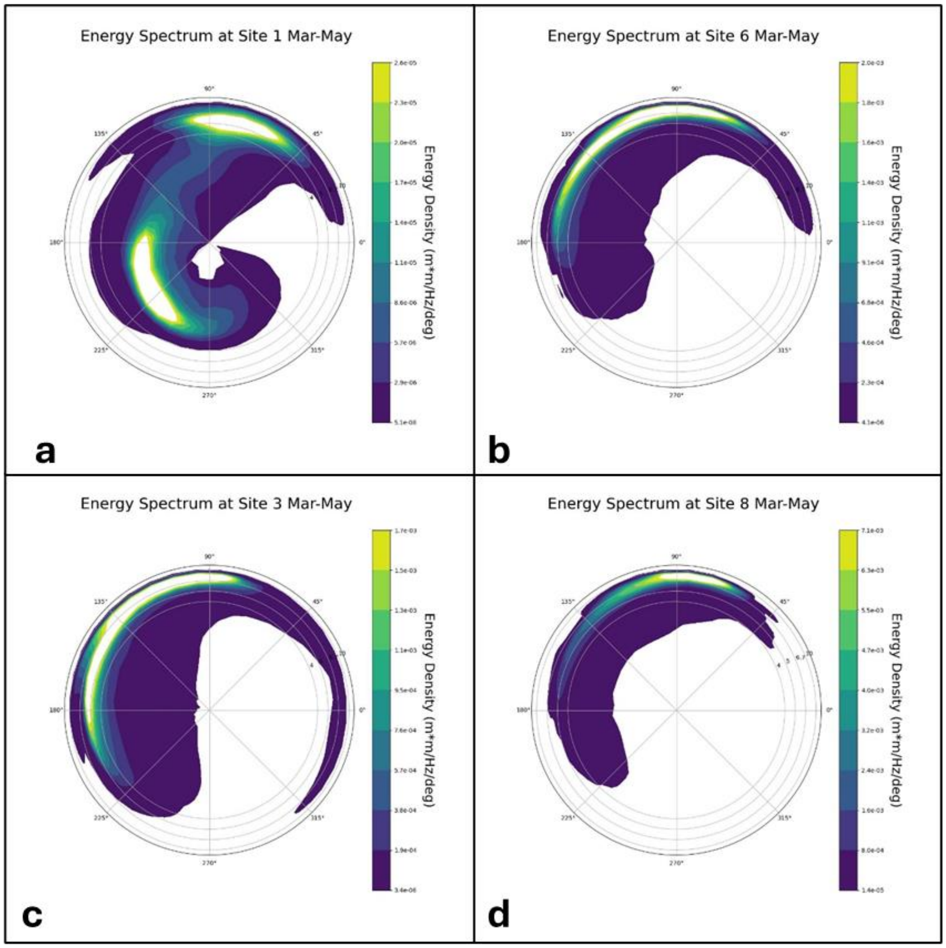

Figure 44 Energy Spectrum During Spring
(a) Station 1, (b) Station 6, (c) Station 3, (d) Station 8

During the summer period shown in Figure 45, the wave energy spectra at Stations 3 and 6 display broad propagation patterns, with most of the energy directed toward the west and northwest. In contrast, at Station 1, wave energy is primarily concentrated toward the southwest, though some energy also propagates northward with lower intensity. The point located south of the study area exhibits a predominant wave energy direction toward the north.

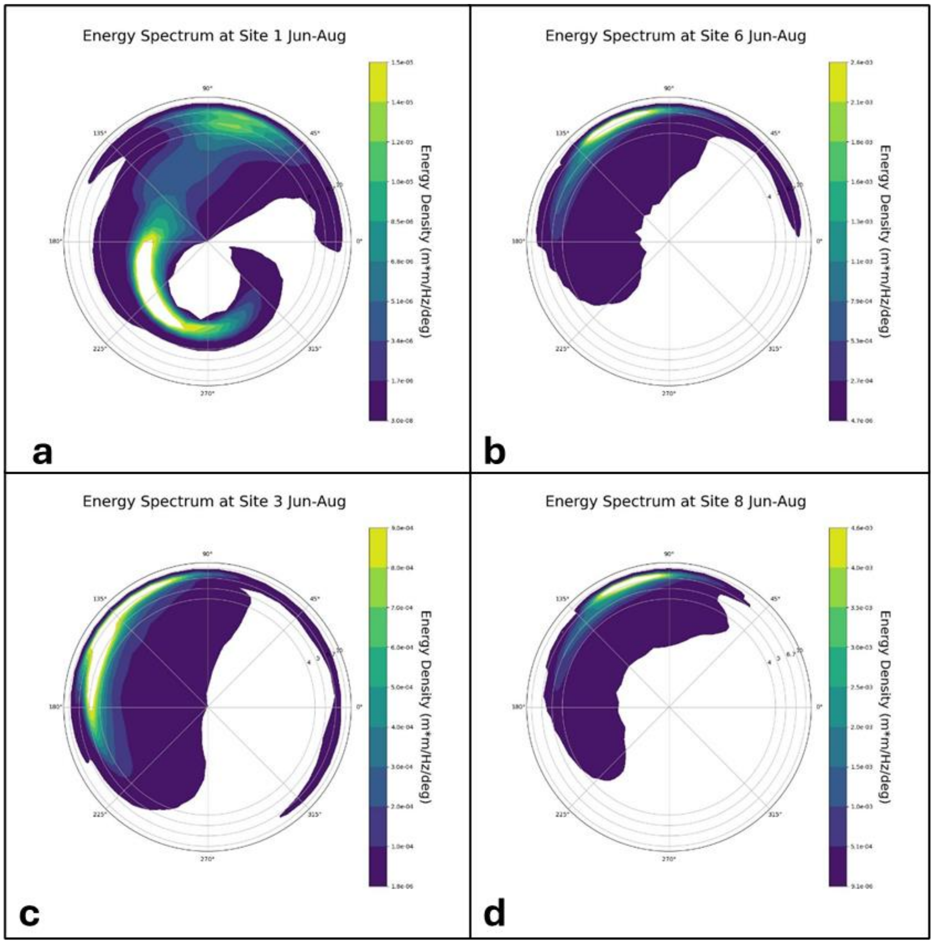

Figure 45 Energy Spectrum During Summer
(a) Station 1, (b) Station 6, (c) Station 3, (d) Station 8

The autumn energy spectrum, as illustrated in Figure 46, reveals distinct directional patterns at the analyzed stations. At Station 1, wave energy is predominantly concentrated toward the north. Stations 6 and 3 exhibit a broader distribution of energy across multiple directions, with stronger intensities directed toward the northwest. At Station 8, the energy spectrum for the autumn season is primarily directed toward the north.

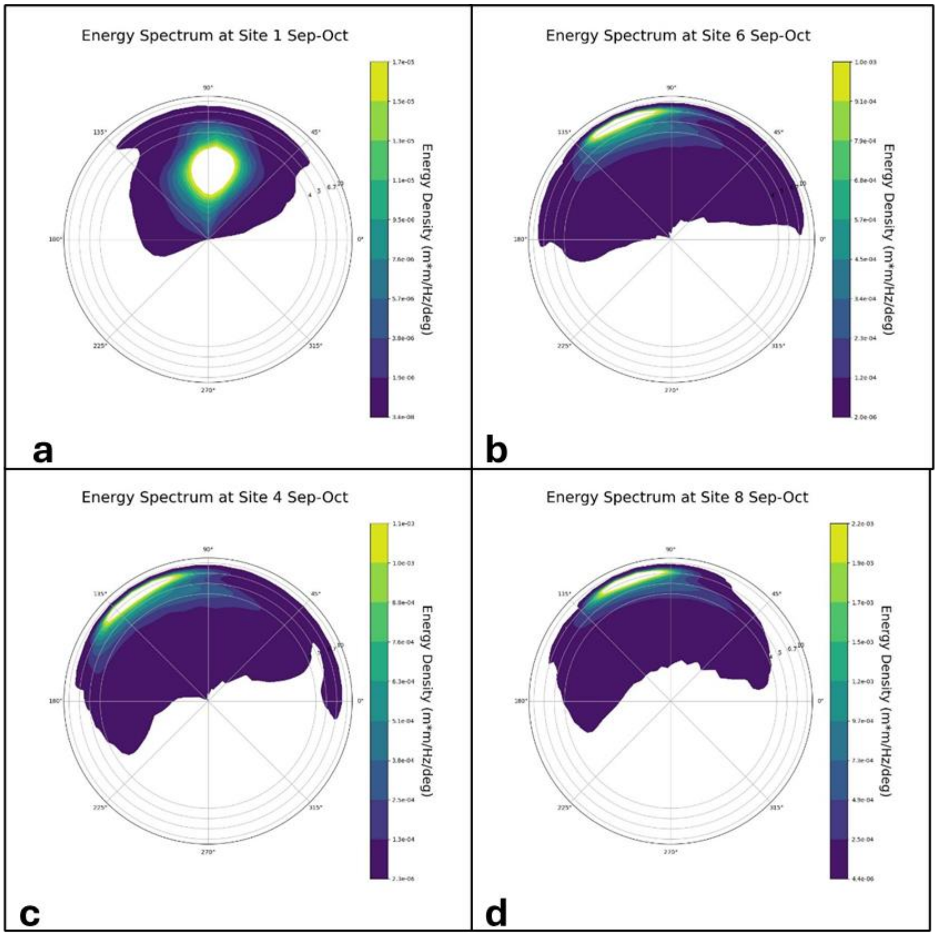

Figure 46 Energy Spectrum During Autumn
(a) Station 1, (b) Station 6, (c) Station 3, (d) Station 8

Early winter energy spectrum in Figure 47 shows that for Station 6 and Station 3 there is a broad distribution, with the highest energy predominantly directed to the north and northwest. Station 1, located at the mouth of the river, has a more concentrated energy distribution that is oriented towards the north. Meanwhile, Station 8, located to the south of the study area, indicates a northward flow of energy during this time of year.

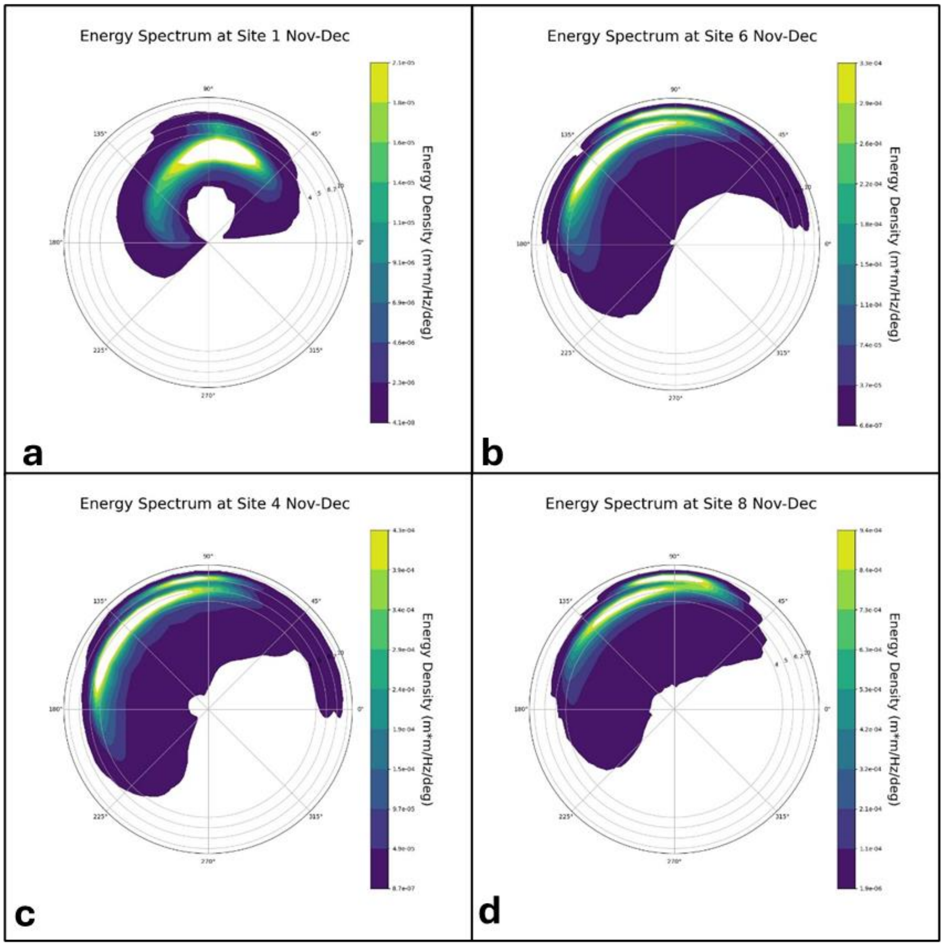

Figure 47 Energy Spectrum at Station 1 Early Winter
(a) Station 1, (b) Station 6, (c) Station 3, (d) Station 8

4.3. Longshore sediment transport – Dredging records

The present study aligns with the framework of Olsen Associates (2002) for estimating littoral transport as the combined volume of maintenance dredging from the outer channel (seaward of station 0+000) and between stations 0+000 to 24+000. This approach is supported by sediment size analyses, which indicate that some sand from the littoral drift enters the inner channel.

Based on 9 years of annual records, the LST corresponds to 955,730 m^3/year (see Table 3).

Table 3 Total Yearly Dredging Volumes Savannah Harbor from channel section 24+000 -50+000 section

Channel Section	2013	2014	2015	2016	2017
-50+000 to -45+000					
-45+000 to -40+000			100,791		
-40+000 to -35+000	4,852	453,615	223,112		
-35+000 to -30+000			244,472	556,882	159,597
-30+000 to -25+000			147,137	51,917	
-25+000 to -20+000	112,559		43,367	38,758	
-20+000 to -15+000		120,704	64,657		
-15+000 to -10+000			216,199		
-10+000 to -5+000					
-5+000 to 0+000					
0+000 to 5+000	244		17,514		80,360
5+000 to 10+000			113,596	1,259	55,519
10+000 to 15+000	19,129		63,444		88,517
15+000 to 20+000	82,208		54,088	35,811	173,689
20+000 to 24+000	83,934			107,770	
TOTAL	**302,926**	**574,319**	**1,288,377**	**792,397**	**557,682**
Channel Section	**2018**	**2019**	**2020**	**2021**	**2022**
-50+000 to -45+000			40,721		
-45+000 to -40+000		173,727			
-40+000 to -35+000	234,553	15,488	341,093		185,545
-35+000 to -30+000					
-30+000 to -25+000			26,530		
-25+000 to -20+000		11,341			
-20+000 to -15+000	206,958	212,780			137,281
-15+000 to -10+000		12,038			
-10+000 to -5+000		39,451		1,939	62,117
-5+000 to 0+000		47,880		1,422	31,038
0+000 to 5+000		13,023	2,662	299,283	126,152
5+000 to 10+000	87,567		45,888	408,852	
10+000 to 15+000	146,198		130,919	579,996	2,759
15+000 to 20+000	548,957		147,370	811,993	
20+000 to 24+000	150,025		8,172	749,887	
TOTAL	**1,374,257**	**525,727**	**743,354**	**2,853,371**	**544,892**

The standard deviation of the total annual dredge volumes is 748,510 cubic meters. This statistic illustrates the dispersion of data points around the mean annual dredge volume of 955,730 cubic meters per year. The significant range in values, from a minimum of 302,926 cubic meters in 2013 to a maximum of 2,853,371 cubic meters in 2021, indicates notable interannual variability in dredge volumes.

4.4. Longshore sediment transport – CERC equation

Based on hydrodynamic and wave modeling, LST was computed using the CERC equation at a series of points within the breaking zone near Tybee Island. The computed LST values were then averaged to estimate three distinct regions: north Tybee Island, northeast Tybee Island, and southeast Tybee Island. These results are presented in Table 4:

Table 4 Computed Net LST for the selected points

Points	**1**	**2**	**3**
Gross southward transport	-141,267	-485,864	-728,080
Gross northward transport	285,869	305,846	119,011
Net transport (m^3/year)	144,601	-180,014	-609,089

Figure 48 Location of Computed LST points

At Point 2, located mid-east of Tybee Island, the net transport was computed at 180,014 m^3/year directed southward. Similarly, at Point 3, situated southeast of the island, the net transport was higher at 609,089 m^3/year, also directed southward. In contrast, point 1, located north of the island, exhibited a net transport rate of 144,601 m^3/year with a northward direction.

The LST rate at Point 2 falls within the estimated range of 100,000 to 300,000 m^3/year for the Georgia coast, as reported by van Gaalen et al. (2016). In South Tybee Island, the calculated LST of 609,089 m^3/year closely aligns with the estimate by Olsen Associates (2002) , who estimated a littoral transport rate of 613,000 m^3/year. The estimated LST rate derived from the dredging records of 955,730 m^3/year for the period between 2013 and 2022 is higher than the computed estimates obtained using the CERC equation. This is to be expected, given that the southward transport decreases at the navigation channel, and the amount of sediment available at Tybee Island is also less.

CHAPTER 5 DISCUSSION

5.1. Hydrodynamics and wave model

The hydrodynamics and waves, as evaluated by the statistical metrics presented in section 4.1. Hydrodynamic and wave modeling, reasonably reproduces the water surface elevation and tides in the study area.

The hydrodynamic model demonstrates a tendency to underestimate water levels throughout all seasons. Nevertheless, it is capable of accurately capturing long-term trends, as evidenced by its high annual Nash-Sutcliffe Efficiency (NSE) of 0.912. However, during periods of rapid water level changes, particularly in spring and autumn, the model is less accurate, as indicated by increased Root Mean Square Error (RMSE) and Scatter Index values. Periods of decreased model accuracy coincide with interseasonal variations.

The SWAN model shows reliable performance in predicting significant wave height results across seasons for both buoys, with summer showing the best accuracy (lowest RMSE and mean bias, and highest NSE) at both locations, indicating reliable model fit during this period. Fall shows the most variability, with higher RMSE and scatter index values, indicating constraints on the model's ability to accurately capture wave dynamics during this season. Spring and early winter maintain moderate accuracy, with slight overestimations reflected in mean bias but stable NSE values, indicating consistent seasonal alignment. Overall, the annual results show stable accuracy with high NSE values (0.731 at buoy 41008, 0.725 at buoy 41112), confirming the long-term reliability of the model.

Sediment dynamics are sensitive to wave energy, direction, and periodic wave patterns, all of which influence sediment transport along coastal and estuarine systems. The performance metrics of the SWAN model (e.g., RMSE, NSE, and Scatter Index) suggest that it is sufficiently accurate for sediment dynamics, especially in summer and early winter when model fit is highest. Seasonal trends of increased error in fall and spring may introduce uncertainties during these periods, potentially affecting the accuracy of short-term sediment transport predictions.

NSE values (>0.7) in the annual analysis at both buoys reflect that the model captures the main patterns and magnitudes of wave heights, which is crucial for understanding sediment behavior throughout the year.

5.2. Energy Spectrum

The seasonal analysis of wave energy spectra across the three stations situated in the vicinity of Tybee Island reveals a predominant energy directionality oriented towards the north and northwest, a trend that is consistently observed across all periods. While some stations display a broad energy distribution across the spectrum, indicating multiple directional components, others exhibit a concentrated peak, suggesting a strong directional focus. Although the results do not clearly delineate periods with solely concentrated or broad energy distribution, the strongest energy flow in each season is regularly directed north and northwest. These findings highlight the complex seasonal wave dynamics that influence sediment transport pathways and energy distribution near Tybee Island and Savannah Channel.

The results are in accordance with the conclusions presented by Oertel et al. (1985), which indicate that waves predominantly transport littoral material from south to north between early spring and mid-fall. This observed northward sediment movement corroborates the findings at the analyzed stations near Tybee Island, where wave energy and sediment transport predominantly follow north and northwest directions across seasons.

However, the predominantly north and northwest energy direction observed at stations located outside of Tybee was expected to show a southward predominant direction, which was not the case. Furthermore, the energy spectrum results do not align with the predominant direction observed in the LST results in points 2 and 3.

5.3. Longshore sediment transport

Material entering the channel, as estimated by 2013-2022 dredging records, provides a localized empirical measurement of sediment transport within the study area. The estimated rate of 955,730 m^3/year is higher than the 613,000 m^3/year estimated by Olsen Associates (2002). However, the estimate by Olsen Associates (2002) falls within the standard deviation of 2013-2022 dredging records, indicating consistency of the estimated sand influx in the channel.

Computed LST at Point 1, shows net northward movement of 144,601 m^3/year. At Points 2 and 3, the trend shifts, with southward transport surpassing northward, leading to net southward transport of 180,014 m^3/year and 609,089 m^3/year, respectively. Southward transport increases significantly from Point 2 to Point 3, while northward LST rates are lower in point 1 compared with points 2 and 3. This indicates a progressively stronger southward littoral drift or sediment transport mechanism towards the south of the outer channel.

Computed LST rates of 144,601 m^3/year northward in point 1 and 180,014 m^3/year southward in point 2, are with the LST rate range estimated by van Gaalen et al. (2016) of 100,000 m^3/y to 300,000 m^3/y. Computed LST rate southeast of Tybee, at 609,089 m^3/year, indicates that more sediment is available to move southward, as the influence of the Savannah River channel diminishes with increasing distance from the channel. This higher value can also be associated with the energy flux method, which relies on wave energy data to estimate sediment transport rates and typically produces higher LST estimates (CERC, 1984). While this trend is not observed for points 1 and 2, it is likely the case for point 3.

5.4. Estimated LST rates with river inputs and dredge records

Previous studies in the Savannah Harbor area, combined with hydrodynamic model, and sediment size analysis presented in this document, indicate that river inflow does not contribute sediment to the outer channel or river mouth. Instead, the outer channel and the inner channel section (from 0+000 to 24+000) are primarily supplied by sediment from offshore sources. Both fine-grained and coarse-grained materials entering the river predominantly originate from the ocean, underscoring the significant role of marine processes in sediment dynamics within this region. As a result, the comparison of riverine sediment inputs with computed LST results will not be included in the present analysis.

Total annual dredging volumes in the outer channel fluctuate significantly, ranging from a low of 117,655 m^3 in 2013 to a peak of 1,057,249 m^3 in 2015. In the outer channel and the section of the inner channel where LST settles, there is also a significant range in values, from a minimum of 302,926 cubic meters in 2013 to a maximum of 2,853,371 cubic meters in 2021.

These fluctuations in dredging volumes demonstrate the natural variability in sediment transport and deposition within the channel, showing that while the results from Olsen Associates (2002) (613,000 m^3/year) and the 2013–2022 dredging records (955,730 m^3/year) differ in magnitude, they are still reasonable and consistent with the variability observed in the system.

The natural sediment dynamics in study area have been altered by the presence of the navigation channel and sediment trapping processes. This disruption results in southward LST being lower at the three computed points compared to the navigation channel, highlighting the channel's significant influence on sediment movement and distribution.

CHAPTER 6 CONCLUSIONS

The present study estimated sand influx into the Savannah River Navigation Channel based on dredging records, conducted hydrodynamic and wave modeling in the study area, and computed longshore sediment transport (LST) rates using the CERC equation. Subsequently, a comparative evaluation of dredging records and computed LST rates was performed.

Riverine inputs were initially sourced from secondary literature. A subsequent literature review and hydrodynamic and wave modelling confirmed that these sediments do not reach the inner channel. Consequently, riverine inputs were excluded from the comparison with computed LST.

The seasonal wave energy analysis conducted near Tybee Island consistently indicates a north-northwest direction. Some stations show a broad energy distribution, while others display a concentrated peak. Despite these variations, the strongest energy flow remains north-northwest. However, the energy spectrum results contrast with the longshore sediment transport, which shows a southward direction.

The sand influx into the outer channel and sections of the inner channel where sand material accumulates, as estimated from dredge records between 2013 and 2022, was compared with the sand influx estimates by Olsen and Associates (2002). While differences in magnitude were observed, the results were found to be statistically consistent. The computed longshore sediment transport (LST) using the CERC equation, however, cannot be directly compared to sand influx derived from dredging records. This is because dredge records include sediment from sections of the outer channel located beyond the breaking zone where the CERC equation is applied. Additionally, computed LST results are specific to areas south of the river channel, where sediment inputs decrease as material becomes trapped in the navigation channel. For this reason, computed LST was instead compared to the estimated LST range reported by van Gaalen et al. (2016).

The calculated LST values are as follows: Point 1 (north of Tybee Island) showed 144,601 m^3/year northward, point 2 (mid-east of Tybee Island) showed 180,014 m^3/year southward, and Point 3 (southeast of Tybee Island) showed 609,089 m^3/year southward. van Gaalen et al. (2016) estimated Georgia's LST rates to be within the range of 100,000 to 300,000 m^3/year. Even though the mentioned study estimates general trends along the Atlantic coast rather than specific in-situ measurements for the Savannah Harbor area, the computed results are within the range in two of the three estimated points.

Material entering the channel, estimated at 955,730 m^3/year from 2013–2022 dredging records, exceeds Olsen Associates (2002) estimate of 613,000 m^3/year. However, as it was mentioned before, Olsen Associates (2002) estimate falls within the standard deviation of the dredging data, demonstrating consistency in the channel's sand influx estimates.

The region spanning latitudes 31° to 32° along the Georgia coast lacks comprehensive LST analysis, with few numerical estimates available. This highlights the need for more detailed and consistent evaluations to better understand sediment transport dynamics in the area.

Further analysis could incorporate the implementation of alternative empirical equations that account for additional parameters, such as beach slope and sediment size. Including these variables would enhance the robustness of the analysis and enable the comparison of results derived from multiple methodologies.

REFERENCES

Appendini, C. M., Salles, P., Mendoza, E. T., López, J., & Torres-Freyermuth, A. (2012). Longshore Sediment Transport on the Northern Coast of the Yucatan Peninsula. *Journal of Coastal Research*, *28*(6), 1404-1417, 1414. https://doi.org/10.2112/JCOASTRES-D-11-00162.1

Aragonés, L., Pagán, J. I., López, I., & Serra, J. C. (2018). Depth of closure: New calculation method based on sediment data. *International Journal of Sediment Research*, *33*(2), 198-207. https://doi.org/https://doi.org/10.1016/j.ijsrc.2017.12.001

ATM. (2002). Savannah Harbor Beach Erosion Study (G. P. AUTHORITY, Trans.). In (pp. 100): GEORGIA PORTS AUTHORITY.

Barua, D. K. (2015). LONGSHORE SAND TRANSPORT -- AN EXAMINATION OF METHODS AND ASSOCIATED UNCERTAINTIES [Article]. *Proceedings of the Coastal Sediments 2015, The*, 1-14. https://search.ebscohost.com/login.aspx?direct=true&AuthType=ip,shib&db=eih&AN=130760018&site=eds-live&custid=uga1

Bayram, A., Larson, M., Hanson, H., & Carr, C. (2007). *A new formula for total longshore transport rate*. https://doi.org/10.1142/9789812709554_0283

Bilskie, M. V., Hagen, S. C., & Medeiros, S. C. (2020). Unstructured finite element mesh decimation for real-time Hurricane storm surge forecasting. *Coastal Engineering*, *156*, 103622. https://doi.org/https://doi.org/10.1016/j.coastaleng.2019.103622

Blanton, B. O., Aretxabaleta, A., Werner, F. E., & Seim, H. E. (2003). Monthly climatology of the continental shelf waters of the South Atlantic Bight. *Journal of Geophysical Research: Oceans*, *108*(C8). https://doi.org/https://doi.org/10.1029/2002JC001609

Blanton, J. O., Garrett, A. J., Bollinger, J. S., Hayes, D. W., Koffman, L. D., & Amft, J. (2009). Transport and Dispersion of a Conservative Tracer in Coastal Waters with Large Intertidal Areas. *Estuaries and Coasts*, *32*(3), 573-592. http://www.jstor.org/stable/40663565

Blanton, J. O., Schwing, F. B., Weber, A. H., Pietrafesa, L. J., & Hayes, D. W. (1985). Wind Stress Climatology in the South Atlantic Bight. In *Oceanography of the Southeastern U.S. Continental Shelf* (pp. 10-22). https://doi.org/https://doi.org/10.1029/CO002p0010

Booij, N., Holthuijsen, L., & Ris, R. (1996). THE "SWAN" WAVE MODEL FOR SHALLOW WATER. *Coastal Engineering*, *1*.

Booij, N., Ris, R., & Holthuijsen, L. (1999a). A third-generation wave model for coastal regions, Part I, Model description and validation. *J. Geophys. Res.*, *104*, 7649-7656.

Booij, N., Ris, R. C., & Holthuijsen, L. H. (1999b). A third-generation wave model for coastal regions: 1. Model description and validation. *Journal of Geophysical Research: Oceans*, *104*(C4), 7649-7666. https://doi.org/https://doi.org/10.1029/98JC02622

Carse, A., & Lewis, J. A. (2020). New horizons for dredging research: The ecology and politics of harbor deepening in the southeastern United States. *WIREs Water*, *7*(6), e1485. https://doi.org/https://doi.org/10.1002/wat2.1485

CERC, C. E. R. C. (1984). *Shore protection manual, volumes I and II.* (U. S. A. C. o. Engineers, Ed. Vol. I, II). Dept. of the Army, Waterways Experiment Station, Corps of Engineers, Coastal Engineering Research Center.

Chempalayil, S. P., Kumar, V. S., Dora, G. U., & Johnson, G. (2014). Near shore waves, long-shore currents and sediment transport along micro-tidal beaches, central west coast of India [Article]. *International Journal of Sediment Research*, *29*(3), 402-413. https://doi.org/10.1016/S1001-6279(14)60054-8

Defne, Z., Haas, K. A., & Fritz, H. M. (2011). Numerical modeling of tidal currents and the effects of power extraction on estuarine hydrodynamics along the Georgia coast, USA.

Renewable Energy, *36*(12), 3461-3471. https://doi.org/https://doi.org/10.1016/j.renene.2011.05.027

Delft. (2024). *SWAN USER MANUAL SWAN Cycle III version 41.45A*. https://swanmodel.sourceforge.io/download/zip/swanuse.pdf

Demirbilek, Z., & Linwood, C. (2002). Coastal engineering manual. *US Army Corps of Engineers, USACE*.

Dietrich, J. C., Tanaka, S., Westerink, J. J., Dawson, C. N., Luettich, R. A., Zijlema, M., Holthuijsen, L. H., Smith, J. M., Westerink, L. G., & Westerink, H. J. (2012). Performance of the Unstructured-Mesh, SWAN+ADCIRC Model in Computing Hurricane Waves and Surge. *Journal of Scientific Computing*, *52*(2), 468-497. https://doi.org/10.1007/s10915-011-9555-6

Dietrich, J. C., Zijlema, M., Westerink, J. J., Holthuijsen, L. H., Dawson, C., Luettich, R. A., Jensen, R. E., Smith, J. M., Stelling, G. S., & Stone, G. W. (2011). Modeling hurricane waves and storm surge using integrally-coupled, scalable computations. *Coastal Engineering*, *58*(1), 45-65. https://doi.org/https://doi.org/10.1016/j.coastaleng.2010.08.001

ECMWF. (2024). *ERA5: Data documentation*. European Centre for Medium-Range Weather Forecasts.

Edwards, K. P., Hare, J. A., Werner, F. E., & Blanton, B. O. (2006). Lagrangian circulation on the Southeast US Continental Shelf: Implications for larval dispersal and retention. *Continental Shelf Research*, *26*(12), 1375-1394. https://doi.org/https://doi.org/10.1016/j.csr.2006.01.020

Elko, N., Briggs, T. R., Benedet, L., Robertson, Q., Thomson, G., Webb, B. M., & Garvey, K. (2021). A century of U.S. beach nourishment [Article]. *Ocean and Coastal Management*, *199*. https://doi.org/10.1016/j.ocecoaman.2020.105406

Esteves, L. S., Williams, J. J., & Lisniowski, M. A. (2009). Measuring and modelling longshore sediment transport. *Estuarine, Coastal and Shelf Science*, *83*(1), 47-59. https://doi.org/https://doi.org/10.1016/j.ecss.2009.03.020

GADNR. (1977). *Geologic Map of Georgia*. Georgia Department of Natural Resources. https://epd.georgia.gov/sites/epd.georgia.gov/files/related_files/site_page/SM-3.PDF

Gailani, J. Z., & Smith, S. J. (2014). Nearshore placement of dredged material to support shoreline stabilisation. Proceedings of the Institution of Civil Engineers-Maritime Engineering,

Georgiou, I. Y., Messina, F., Sakib, M. M., Zou, S., Foster-Martinez, M., Bregman, M., Hein, C. J., Fenster, M. S., Shawler, J. L., McPherran, K., & Trembanis, A. C. (2023). Hydrodynamics and Sediment-Transport Pathways along a Mixed-Energy Spit-Inlet System: A Modeling Study at Chincoteague Inlet (Virginia, USA). *Journal of Marine Science and Engineering*, *11*(5), 1075. https://www.mdpi.com/2077-1312/11/5/1075

Georgiou, I. Y., & Schindler, J. (2009). Chapter H. Numerical simulation of waves and sediment transport along a transgressive barrier island. In D. Lavoie (Ed.), *Sand Resources, Regional Geology, and Coastal Processes of the Chandeleur Islands Coastal System: an Evaluation of the Breton National Wildlife Refuge* (Vol. Report 2009–5252, pp. p. 143–168.). U.S. Geological Survey Scientific Investigations. https://www.sciencedirect.com/science/article/pii/S0025322706001083

Hagen, S., Zundel, A., & Kojima, S. (2006). Automatic, unstructured mesh generation for tidal calculations in a large domain. *International Journal of Computational Fluid Dynamics*, *20*, 593-608. https://doi.org/10.1080/10618560601046846

Hersbach, H., Bell, B., Berrisford, P., Hirahara, S., Horányi, A., Muñoz Sabater, J., Nicolas, J., Peubey, C., Radu, R., Schepers, D., Simmons, A., Soci, C., Abdalla, S., Abellan, X., Balsamo, G., Bechtold, P., Biavati, G., Bidlot, J., Bonavita, M., & Thépaut, J. N. (2020). The ERA5 global reanalysis. *Quarterly Journal of the Royal Meteorological Society*, *146*. https://doi.org/10.1002/qj.3803

Hudson, A., Moritz, H. R., Norton, J., Research, E., Center, D., Coastal, Laboratory, H., & Program, N. R. S. M. (2022). *Sediment Mobility, Closure Depth, and the Littoral System – Oregon and Washington Coast*. U.S. Army Engineer Research and Development Center, [Coastal and Hydraulics Laboratory]. https://books.google.com/books?id=i2RizwEACAAJ

Jones, M. C., Bernhardt, C. E., Krauss, K. W., & Noe, G. B. (2017). The Impact of Late Holocene Land Use Change, Climate Variability, and Sea Level Rise on Carbon Storage in Tidal Freshwater Wetlands on the Southeastern United States Coastal Plain. *Journal of Geophysical Research: Biogeosciences*, *122*(12), 3126-3141. https://doi.org/https://doi.org/10.1002/2017JG004015

Kamphuis, J. W. (1991). Alongshore Sediment Transport Rate. *Journal of Waterway, Port, Coastal, and Ocean Engineering*, *117*(6), 624-640. https://doi.org/doi:10.1061/(ASCE)0733-950X(1991)117:6(624)

Komar, P. D., & Inman, D. L. (1970). Longshore sand transport on beaches. *Journal of Geophysical Research (1896-1977)*, *75*(30), 5914-5927. https://doi.org/https://doi.org/10.1029/JC075i030p05914

Kress, M. M., Touzinsky, K. F., Vuxton, E. A., Greenfeld, B., Lillycrop, L. S., & Rosati, J. D. (2016). Alignment of U. S. ACE Civil Works Missions to Restore Habitat and Increase Environmental Resiliency. *Coastal Management*, *44*(3), 193-208. https://doi.org/10.1080/08920753.2016.1160203

Lobeto, H., Menendez, M., Losada, I. J., & Hemer, M. (2022). The effect of climate change on wind-wave directional spectra. *Global and Planetary Change*, *213*, 103820. https://doi.org/https://doi.org/10.1016/j.gloplacha.2022.103820

Lucas, C., Boukhanovsky, A., & Guedes Soares, C. (2011). Modeling the climatic variability of directional wave spectra. *Ocean Engineering*, *38*(11), 1283-1290. https://doi.org/https://doi.org/10.1016/j.oceaneng.2011.04.003

Luettich, J. R., & Westerink, J. (2004). Formulation and Numerical Implementation of the 2D/3D ADCIRC Finite Element Model Version 44.XX.

Luettich, J. R., Westerink, J., & Scheffner, N. (1992). ADCIRC: An Advanced Three-Dimensional Circulation Model for Shelves, Coasts, and Estuaries. Report 1. Theory and Methodology of ADCIRC-2DDI and ADCIRC-3DL. *Dredging Research Program Tech. Rep. DRP-92-6*, 143.

Luettich, R. A., Westerink, J. J., & Texas Water Development, B. (2004). *Formulation and numerical implementation of the 2D/3D ADCIRC finite element model version 44. XX*. [R. Luettich?].

Meyer, B. K., Vance, R. K., Bishop, G. A., & Dai, D. (2016). Shoreline dynamics and environmental change under the modern marine transgression; St. Catherines Island, Georgia, USA. *Environmental Earth Sciences*, *75*(1). https://doi.org/10.1007/s12665-015-4780-1

Michel, J. M. (2013). *South Atlantic information resources: data search and literature synthesis*. US Department of the Interior, Bureau of Ocean Energy Management, Gulf of ….

Mil-Homens, J., Ranasinghe, R., van Thiel de Vries, J. S. M., & Stive, M. J. F. (2013). Re-evaluation and improvement of three commonly used bulk longshore sediment transport formulas. *Coastal Engineering*, *75*, 29-39. https://doi.org/https://doi.org/10.1016/j.coastaleng.2013.01.004

Mulholland, P. J., & Olsen, C. R. (1992). Marine origin of Savannah River estuary sediments: Evidence from radioactive and stable isotope tracers. *Estuarine, Coastal and Shelf Science*, *34*(1), 95-107. https://doi.org/https://doi.org/10.1016/S0272-7714(05)80129-5

Oertel, G. F., Fowler, J. E., & Pope, J. (1985). *History of erosion and erosion control efforts at Tybee Island, Georgia*. US Army Engineer Waterways Experiment Station.

Olsen Associates, I. (2002). Review Comments Regarding "Draft-Savannah Harbor Beach Erosion Study (October 2001).

Applied Technology & Management (ATM). In (pp. 15): Olsen Associates, Inc.

Ouillon, S. (2019). *Sediment Transport in Coastal Waters* [Online
Non-fiction
Electronic document]. MDPI - Multidisciplinary Digital Publishing Institute. https://search.ebscohost.com/login.aspx?direct=true&AuthType=ip,shib&db=cat06564a&AN=uga.9922343461902931&site=eds-live&custid=uga1
https://galileo-uga.primo.exlibrisgroup.com/openurl/01GALI_UGA/01GALI_UGA:UGA?u.ignore_date_coverage=true&rft.mms_id=9922343461902931

Palaparthi, J., & Briggs, T. R. (2024). Regional Sediment Management in US Coastal States: Historical Trends and Future Predictions. *Journal of Marine Science and Engineering*, *12*(4), 528. https://www.mdpi.com/2077-1312/12/4/528

Pandoe, W. W., & Edge, B. L. (2008). Case Study for a Cohesive Sediment Transport Model for Matagorda Bay, Texas, with Coupled ADCIRC 2D-Transport and SWAN Wave Models. *Journal of Hydraulic Engineering*, *134*(3), 303-314. https://doi.org/doi:10.1061/(ASCE)0733-9429(2008)134:3(303)

Papanicolaou, A. N., Elhakeem, M., Krallis, G., Prakash, S., & Edinger, J. (2008). Sediment Transport Modeling Review—Current and Future Developments. *Journal of Hydraulic Engineering*, *134*(1), 1-14. https://doi.org/doi:10.1061/(ASCE)0733-9429(2008)134:1(1)

Ramos, S. J. (2014). Planning for competitive port expansion on the U.S. Eastern Seaboard: the case of the Savannah Harbor Expansion Project [Article]. *Journal of Transport Geography*, *36*, 32-41. https://doi.org/10.1016/j.jtrangeo.2014.02.007

Reeve, D., Chadwick, A. J., & Fleming, C. (2018). *Coastal engineering : process, theory and design practice* (Third edition. ed.). CRC Press.

Salem Cherif, Y., Mezouar, K., Guerfi, M., Sallaye, M., & Dahmani, A. E. A. (2019). Nearshore hydrodynamics and sediment transport processes along the sandy coast of Boumerdes, Algeria. *Arabian Journal of Geosciences*, *12*(24), 800. https://doi.org/10.1007/s12517-019-4981-0

Seymour, R. J. (2005). Longshore Sediment Transport. In M. L. Schwartz (Ed.), *Encyclopedia of Coastal Science* (pp. 600-600). Springer Netherlands. https://doi.org/10.1007/1-4020-3880-1_199

Shaeri, S., Etemad-Shahidi, A., & Tomlinson, R. (2020). Revisiting Longshore Sediment Transport Formulas. *JOURNAL OF WATERWAY PORT COASTAL AND OCEAN ENGINEERING*, *146*(4), 04020009. https://doi.org/10.1061/(ASCE)WW.1943-5460.0000557

SKIO. (2022). *Georgia Coastal Hazards Portal* [Georgia Coastal Hazards Portal]. https://doi.org/https://www.arcgis.com/home/item.html?id=2e2d61fad5d44e0c96995c38feb7052d

Smith, E. R., Wang, P., Ebersole, B. A., & Zhang, J. (2009). Dependence of Total Longshore Sediment Transport Rates on Incident Wave Parameters and Breaker Type. *Journal of Coastal Research*, *25*(3), 675-683. http://www.jstor.org/stable/27698361

Smith, J. M., Stauble, D. K., P., W. B., & J., W. M. (2008). *Impact of Savannah Harbor Deep Draft Navigation Project on Tybee Island Shelf and Shoreline*. U.S. Army Engineer Research and Development Center, Coastal and Hydraulics Laboratory.

Sytsma C., Jackson R, Risse M., Kurth M., Alexander C., Bilskie M., Villegas O., & E., K. (2023). Coastal Sediment Budgeting to Match Sediment Suppluies, Dredging Volumes, And Natural Infrastructure Enhancement Needs for Sea-Level Rise Adaptation. In U. A. C. o. E. UGA, Engineer Research and Development Center, (Ed.).

Tomasicchio, G. R., D'Alessandro, F., Barbaro, G., & Malara, G. (2013). General longshore transport model. *Coastal Engineering*, *71*, 28-36. https://doi.org/10.1016/j.coastaleng.2012.07.004

Trombetta, T. B., Marques, W. C., Guimarães, R. C., & Costi, J. (2020). An overview of longshore sediment transport on the Brazilian coast. *Regional Studies in Marine Science*, *35*, 101099. https://doi.org/https://doi.org/10.1016/j.rsma.2020.101099

USACE. (2002a). *CEM: Coastal Engineering Manual*. U.S. Army Corps of Engineers. https://books.google.com/books?id=QLO_jwEACAAJ

USACE. (2002b). *Dredged Material Physical Analysis Report*.

USACE. (2009). *Sedimentation Analysus - Final Environmental Impact Statement for Savannah Harbor Expansion Project* (Sedimentation Analysis, Issue.

USACE. (2012). *Final Environmental Impact Statement: Savannah Harbor Expansion Project.*: U.S. Army Corps of Engineers Retrieved from https://www.sas.usace.army.mil/Portals/61/docs/SHEP/Reports/EIS/Abstract%20SHEP%20FINAL%20EIS.pdf

USACE. (2015). *Dredging and Dredged Material Management*. U.S. Army Corps of Engineers

USACE. (2023). Expanding Beneficial Use of Dredged Material in USACE. In U. S. A. C. o. Engineers (Ed.): U.S. Army Corps of Engineers.

USACE. (2024a). *Savannah Harbor Expansion*. U.S. Army Corps of Engineers. Retrieved 02/15/2024 from

USACE. (2024b). *Savannah Harbor Maintenance*. U.S. Army Corps of Engineers

USACE, U. A. C. (2020). *2020 South Atlantic Division Regional Sediment Management Optimization Update*.

USDOT. (2024). Port Profiles. In: U.S. Department of Transportation (USDOT).

USGS. (2019). *The National Map—New data delivery homepage, advanced viewer, lidar visualization* [Report](2019-3032). (Fact Sheet, Issue. U. S. G. Survey. https://pubs.usgs.gov/publication/fs20193032

Valiente, N. G., Masselink, G., Scott, T., Conley, D., & McCarroll, R. J. (2019). Role of waves and tides on depth of closure and potential for headland bypassing. *Marine Geology*, *407*, 60-75. https://doi.org/https://doi.org/10.1016/j.margeo.2018.10.009

van Gaalen, J. F., Tebbens, S. F., & Barton, C. C. (2016). Longshore Sediment Transport Directions and Rates from Northern Maine to Tampa Bay, Florida: Literature Compilation and Interpretation [research-article]. *Journal of Coastal Research*, *32*(6), 1277-1301. https://search.ebscohost.com/login.aspx?direct=true&AuthType=ip,shib&db=edsjsr&AN=edsjsr.44028224&site=eds-live&custid=uga1

van Rijn, L. C. (2014). A simple general expression for longshore transport of sand, gravel and shingle [Article]. *Coastal Engineering*, *90*, 23-39. https://doi.org/10.1016/j.coastaleng.2014.04.008

Williams, J. J., Esteves, L. S., Lisniowski, M. A., & Perotto, H. L. S. (2007). Field Measurements and Modelling of Longshore Sediment Transport. In *Coastal Sediments '07* (pp. 221-234). https://doi.org/doi:10.1061/40926(239)17

Zijlema, M. (2010). Computation of wind-wave spectra in coastal waters with SWAN on unstructured grids. *Coastal Engineering*, *57*(3), 267-277. https://doi.org/https://doi.org/10.1016/j.coastaleng.2009.10.011